

CoMaL: Conditional Maximum Likelihood Approach to Self-supervised Domain Adaptation in Long-tail Semantic Segmentation

Thanh-Dat Truong¹ *Student Member, IEEE*, Chi Nhan Duong² *Member, IEEE*, Pierce Helton¹, Ashley Dowling³,
Xin Li⁴ *Fellow, IEEE*, Khoa Luu¹ *Member, IEEE*,

Abstract—The research in self-supervised domain adaptation in semantic segmentation has recently received considerable attention. Although GAN-based methods have become one of the most popular approaches to domain adaptation, they have suffered from some limitations. They are insufficient to model both global and local structures of a given image, especially in small regions of tail classes. Moreover, they perform bad on the tail classes containing limited number of pixels or less training samples. In order to address these issues, we present a new self-supervised domain adaptation approach to tackle long-tail semantic segmentation in this paper. Firstly, a new metric is introduced to formulate long-tail domain adaptation in the segmentation problem. Secondly, a new Conditional Maximum Likelihood (CoMaL) approach¹ in an autoregressive framework is presented to solve the problem of long-tail domain adaptation. Although other segmentation methods work under the pixel independence assumption, the long-tailed pixel distributions in CoMaL are generally solved in the context of structural dependency, as that is more realistic. Finally, the proposed method is evaluated on popular large-scale semantic segmentation benchmarks, i.e., “SYNTHIA → Cityscapes” and “GTA → Cityscapes”, and outperforms the prior methods by a large margin in both the standard and the proposed evaluation protocols.

I. INTRODUCTION

Semantic scene segmentation has become one of the most popular topics in computer vision. It aims to densely assign each pixel in a given image to the corresponding predefined class. Recently, deep learning-based approaches have achieved remarkable results in semantic segmentation [1]–[3]. A typical segmentation method is usually trained on scene datasets with labels. However, annotating images for the semantic segmentation task is costly and time-consuming, since it requires every single pixel in a given image to be labeled. Another approach of reducing the cost of annotating images is to use a simulation to create a large-scale synthetic dataset [4], [5]. However, deploying the supervised models trained on synthetic datasets to real images is not an appropriate solution, since these supervised models often perform worse on the real images because of a pixel appearance gap between synthetic and real images.

¹Department of Computer Science and Computer Engineering, University of Arkansas; ²Department of Computer Science and Software Engineering, Concordia University, Concordia University; ³Department of Entomology and Plant Pathology, University of Arkansas; and ⁴Lane Department of Computer Science and Electrical Engineering, West Virginia University. Emails: tt032@uark.edu, dcnhan@ieee.org, pchelton@email.uark.edu, adowling@uark.edu, Xin.Li@mail.wvu.edu, khoaluu@uark.edu

¹The source code implementation of CoMaL will be publicly available.

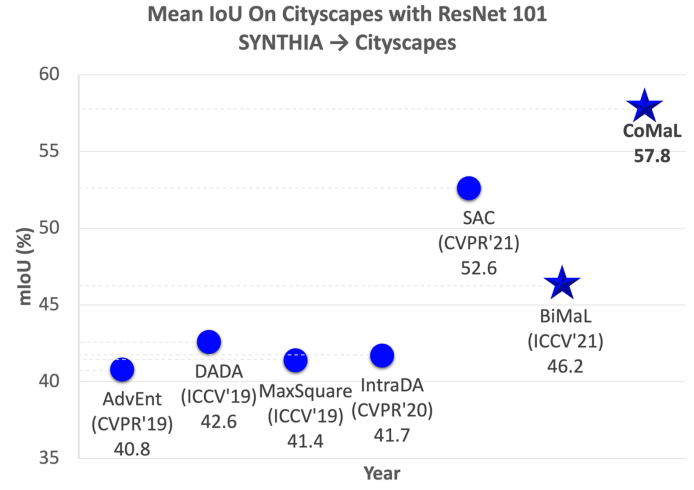


Fig. 1. Overview of Results. The figure illustrates the mIoU results on Cityscapes. Our CoMaL and BiMaL approach achieves the State-of-the-Art results and outperforms prior methods by a large margin.

Self-supervised Domain Adaptation (SDA) aims to learn a model on the annotated source datasets and adapt to unlabeled target datasets to guarantee its performance on the new domain. Common domain adaptation methods usually minimize the distribution discrepancy of the deep representations extracted from the source and target domains in addition to supervised training on the source domain [6]–[9]. The discrepancy minimization can be processed at single or multiple levels of deep feature representation using maximum mean discrepancy [10], [11], adversarial training [7], [12]–[15], or contrastive learning [16], [17]. They have shown their potential performance in aligning the predicted outputs across domains. Another self-training approach that utilizes pseudo labels [18]–[20] on the target domain has also drawn much attention in recent years.

Although these prior methods have shown their high performance in domain adaptation for semantic segmentation, they are still unable to perform well on the tail classes that have limited numbers of pixels, i.e. intra long-tail classes, or less training samples, i.e. inter long-tail classes. As shown in Fig. 2, the number of pixels in classes such as bicycles, traffic signs, and traffic light are limited compared to other classes like road, building, and sky. Although the performance of the trained model on the tailed class in the source domain is reasonable,

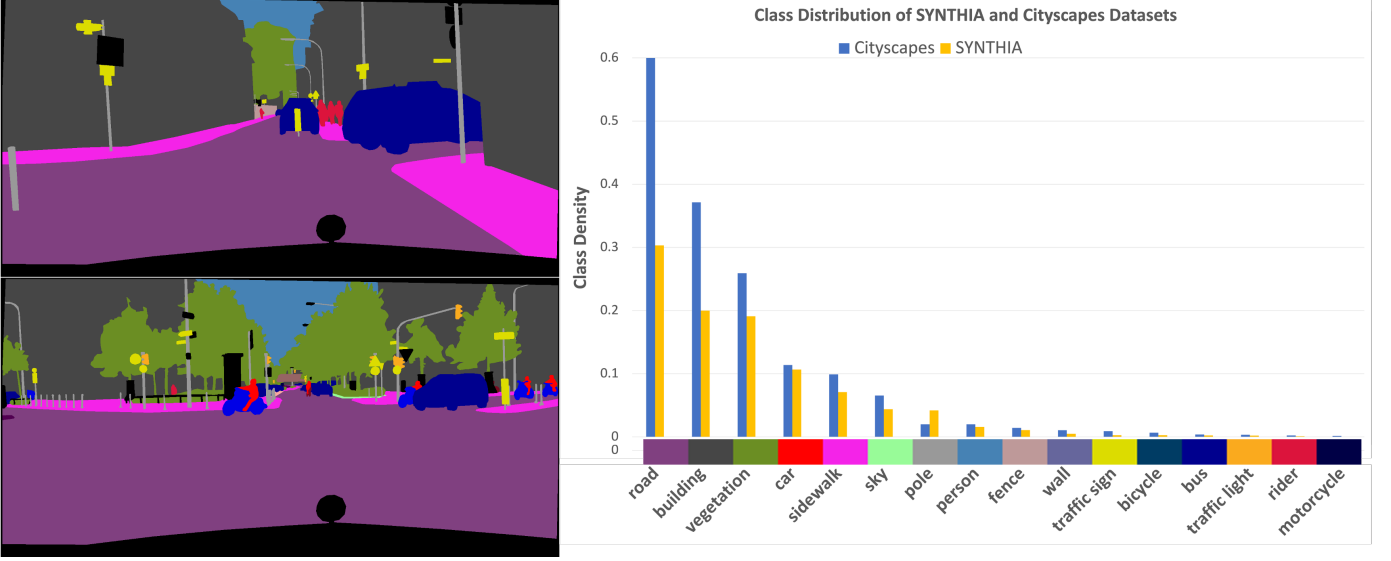


Fig. 2. **The class distributions of SYNTHIA and Cityscapes datasets.** The left figure illustrates the typical segmentation ground-truths of the Cityscapes. The right image show the class distribution over the entire datasets of Cityscapes and SYNTHIA, respectively. Best view in color.

its performance on the tailed classes in the target domain dramatically drops (see Table III). In adversarial methods [6], [7], [21], the learned discriminator usually provides a weak indication of structural learning for the semantic segmentation due to the binary cross-entropy predictions between source and target domains. As a result, they are insufficient in the global and the local structures of a given image, especially in small regions of the tail class. Another entropy metric has been proposed in self-training methods [8], [22] to improve the prediction confidence. However, this metric tends to highly response to the head classes that are usually occupy a lot of pixels in an image rather than tail classes which contribute very limited number of pixels. More importantly, an assumption of *pixel independence* is required for the metric to be applicable. **Contributions of This Work.** This work presents a new self-supervised domain adaptation approach to long-tail semantic scene segmentation, which is an extension of our previous work [23]. In that work, we introduced a new Unaligned Domain Score to measure the efficiency of a learned model on a new target domain in unsupervised manner, and presented a new Bijective Maximum Likelihood (BiMaL) loss that is a generalized form of the Adversarial Entropy Minimization without any assumption about pixel independence. In this work, we further address the long-tail issue that occurs in both labeled source domain **and** new **unlabeled** target domains (as shown in Fig. 2). Unlike prior works where only labeled part is on their focus to alleviate the long-tail problem, our motivation is to address this issue in **both two domains** which is novel and more challenging. Table I summarizes the difference between the proposed and prior methods. The contributions of the paper are four-fold.

- **Firstly, a new metric is formulated for domain adaptation in long-tail semantic segmentation.** Via the proposed metric, several constraints are introduced to the learning process including (1) *multiple predictions per image* (i.e., one class per pixel) with class-balanced

constraint; (2) *local and global constraints via structural learning* with the novel conditional maximum likelihood loss.

- **Secondly, a Bijective Maximum Likelihood (BiMaL) loss** is formed using a Maximum-likelihood formulation to model the global structure of a segmentation input and a Bijective function to map that segmentation structure to a deep latent space. The proposed BiMaL loss can be used with an unsupervised deep neural network to generalize on target domains.
- **Thirdly, a new Conditional Maximum Likelihood (CoMaL) approach** is introduced in the self-supervised domain adaptation framework to tackle the long-tail semantic scene segmentation problem. In this framework, the assumptions of pixel independence made by prior semantic segmentation methods are relaxed while more structural dependencies are efficiently taken into account.
- **Finally,** the proposed BiMaL and CoMaL methods are evaluated on two popular large-scale visual semantic scene segmentation adaptation benchmarks, i.e., SYNTHIA to Cityscapes and GTA to Cityscapes, and **outperforms the prior segmentation methods by a large margin**.

Figure 1 illustrates our state-of-the-art (SOTA) performance compared to prior approaches.

II. RELATED WORK

Domain Adaptation has become one of the most popular research topics due to its ability to ease the notorious requirement of large amounts of labeled data in Computer Vision applications, especially those using deep learning methods. Domain discrepancy minimization [10], [11], [15], adversarial learning [7], [12]–[14], [21], [28], entropy minimization [8], [22], [29], [30], and self-training [20] are the four primary approaches to Domain Adaptation.

TABLE I

COMPARISON IN PROPERTIES BETWEEN OUR APPROACHES AND OTHERS. CONVOLUTIONAL NEURAL NETWORK (CNN), GENERATIVE ADVERSARIAL NET (GAN), BIJECTIVE NETWORK (BiN), MULTI-HEAD ATTENTION NETWORK (MHA), ENTROPY MINIMIZATION (ENTMIN), SEGMENTATION MAP (SEG), DEPTH MAP (DEPTH); ℓ_{IW} : IMAGE-WISE WEIGHTING LOSS, ℓ_{CE} : CROSS-ENTROPY LOSS, ℓ_{Focal} : FOCAL LOSS ℓ_{adv} : ADVERSARIAL LOSS, ℓ_{Huber} : HUBER LOSS. ℓ_{square} : MAXIMUM SQUARES LOSS, $\ell_{density}$: MAXIMUM LIKELIHOOD LOSS, ℓ_{CoMal} : CONDITIONAL MAXIMUM LIKELIHOOD LOSS, ℓ_{Seesaw} : SEESAW LOSS, $\ell_{DropLoss}$: DROP LOSS

Methods	Long-Tail Aware	Long-Tail Level	Structural Learning	Source Label	Target Domain Transfer	Architecture	Designed Loss
AdaptPatch [6]	X	–	Weak (Binary label)	Seg	✓	CNN+GAN	ℓ_{adv}
CBST [20]	X	–	–	Seg	✓	CNN	ℓ_{CE}
ADVENT [8]	X	–	Weak (Binary label)	Seg	✓	CNN+GAN	EntMin+ ℓ_{adv}
IntraDA [22]	X	–	Weak (Binary label)	Seg	✓	CNN+GAN	EntMin+ ℓ_{adv}
Seesaw [24]	✓	Instance	–	–	X	CNN	ℓ_{Seesaw}
DropLoss [25]	✓	Instance	–	–	X	CNN	$\ell_{DropLoss}$
SPIGAN [26]	X	–	Weak (Binary label)	Seg + Depth	✓	CNN+GAN	ℓ_{adv}
DADA [9]	X	–	Depth-aware Label	Seg + Depth	✓	CNN+GAN	$\ell_{adv} + \ell_{Huber}$
MaxSquare [27]	Partial	Semantic	Weak (Binary label)	Seg	✓	CNN + GAN	$\ell_{square} + \ell_{IW}$
SAC [19]	✓	Semantic	–	Seg	✓	CNN	$\ell_{CE} + \ell_{Focal}$
BiMaL	X	–	Maximum Likelihood	Seg	✓	CNN + BiN	$\ell_{density}$
CoMaL	✓	Semantic	Conditional Maximum Likelihood	Seg	✓	CNN + MHA	ℓ_{CoMal}

Semantic Segmentation. The performance provided by Fully Convolutional Networks in semantic segmentation applications makes them the most popular choice for the task, and the accuracy of FCNs improves further when incorporated with an encoder-decoder structure. Some of the first FCN applications [1], [31] segmented images by incorporating spatial pooling after multiple convolutional layers. Works that followed [32], [33] gathered more overall information and maintained accurate instance borders by combining upsampled, high-level feature maps with low-level feature maps prior to decoding. Alternative approaches [1], [34] have utilized dilated convolutions to improve the efficiency of models without sacrificing the field of view. Spatial pyramid pooling has been used by other recent works [2], [35] to obtain contextual information at multiple levels. This approach grants more global information at higher layers in the network. Deeplabv3+ [2] combined spatial pyramid pooling and the encoder-decoder structure in a new, efficient FCN architecture. Recent works have utilized Transformer-based backbones [3], [36], [37] to learn a powerful semantic segmentation network.

Adversarial Training Methods. The approaches in this category are the preferred approaches of utilizing domain adaptation in semantic scene segmentation. The supervised segmentation training on the source domain and the adversarial training are designed in parallel. The first GAN-based approach to semantic segmentation that utilized SDA was introduced by Hoffman et. al. [21]. Chen et. al. [28] made use of pseudo labels in conjunction with global and class-wise adaptation to improve their adversarial learning results. Chen et. al. [12] integrated target-guided distillation loss with a spatial-aware model to learn the real image style and spatial structures of urban scenes. Hong et. al. [14] trained a conditional generator to reproduce features in real images to minimize the gap between these two domains. Tsai et. al. [7] focused on the shared structures between these two domains, using adversarial training to predict similar label distributions across the source and target domains. Other methods have investigated the efficacy of using generative

networks to translate from a conditioned source to a novel target [29], [30]. Hoffman et. al. [13] developed a Cycle-Consistent Adversarial network to adapt representations at the pixel and feature level. Zhu et. al. [38] presented a conservative loss function to promote moderate source examples, while avoiding the extreme examples during adversarial training. Wu et. al. [39] utilized channel-wise alignment during generation and segmentation to further reduce domain shift. Sakardis et. al. [40] introduced a framework to segment foggy city images by gradually training on light, synthetic fog before moving to dense, real fog. Vapnik et. al. [41] was the first to demonstrate the benefits of privileged information over traditional learning methods, granting additional data during training. Privileged information has been widely used since Vapnik’s discovery [42]–[45] to improve model results. SPIGAN [26] made use of privileged information to train a SDA model for semantic segmentation. Vu et. al. [9] created a depth-aware SDA framework to use privileged depth information, similar to SPIGAN.

Entropy Minimization Methods. These approaches have become the preferred approach for semi-supervised learning [46], [47]. Vu et. al. [8] pioneered the use of entropy minimization in semantic segmentation with domain adaptation: adversarial learning further improves the results of the minimization process. Using the entropy level of prediction, [22], [48] created an intradomain adaptation approach with two learning phases. The first phase performs the standard adaptation from the source to target domain, while the second aligns the easy and hard split in the target domain. Truong et. al. [23] introduced a novel bijective maximum likelihood approach to domain adaptation, which is a general form of entropy minimization to learn the global structure of the segmentation. Self-training is another recently developed domain adaptation method for segmentation [19], [20] and classification [49]. In self-training, a new model is trained on unlabeled data by using pseudolabels derived from predictions of a trained model.

Long-tail Recognition. Ziwei et. al. [50] presented Open Long-tail Recognition to handle imbalanced classification, few-shot learning, and open-set recognition. They developed

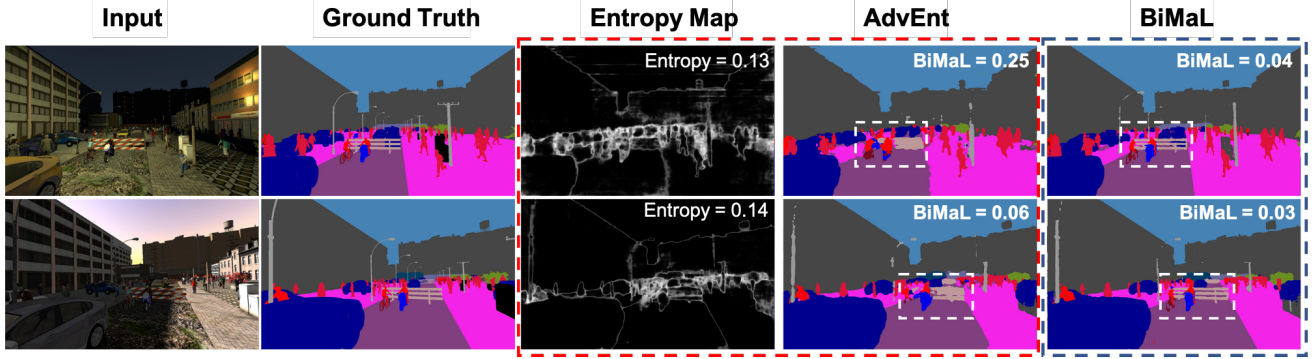


Fig. 3. Two images have the same entropy but one has a poor prediction (a top image) and one has a better prediction (a bottom image). Columns 1 and 2 are an input image and a ground truth. Columns 3 and 4 are an entropy map and a prediction of AdvEnt [8]. Column 5 is the results of our proposed method. The two predictions produced by AdvEnt have similar entropy scores (0.13 and 0.14). Meanwhile, the BiMaL value of the bottom prediction (0.06) is smaller than the top prediction (0.14). Our results in the last column, which have better BiMaL values than AdvEnt, can well model the structure of an image. In particular, our results have sharper results of a barrier and a rider (white dash box), and a clear boundary between road and sidewalk.

an integrated algorithm that transforms an image to a feature space, and their dynamic meta-embedding combines a direct image feature and a related memory feature, where the feature norm displays the familiarity of known classes. Jiawei et al. [51] introduced Balanced Softmax, an unbiased extension of Softmax, to facilitate the distribution shift of labels between training and testing. Moreover, they introduced Balanced Meta-Softmax to enhance the long-tail learning by applying a complementary meta-sampler to estimate the optimal class sample rate. Wang et al. [24] introduced seesaw loss to rebalance the fairness of gradients produced by positive and negative samples of a class with two regularization terms, i.e. mitigation and compensation.

III. CROSS-DOMAIN ADAPTATION FOR SEMANTIC SEGMENTATION

Let $\mathbf{x}_s \in \mathcal{X}_s \subset \mathbb{R}^{H \times W \times 3}$ be an input image of the source domain (H and W are the height and width of an image), $\mathbf{x}_t \in \mathcal{X}_t \subset \mathbb{R}^{H \times W \times 3}$ be an input image of the target domain, $F : \mathcal{X} \rightarrow \mathcal{Y}$ where $\mathcal{X} = \mathcal{X}_s \cup \mathcal{X}_t$ be a semantic segmentation function that maps an input image to its corresponding segmentation map $\mathbf{y} \in \mathbb{R}^{H \times W \times C}$, i.e. $\mathbf{y} = F(\mathbf{x}, \theta)$ (C is the number of semantic classes). In general, given N_s labeled training samples from a source domain $\mathcal{D}_s = \{\mathbf{x}_s^i, \hat{\mathbf{y}}_s^i\}_{i=1}^{N_s}$ and N_t unlabeled samples from a target domain $\mathcal{D}_t = \{\mathbf{x}_t^i\}_{i=1}^{N_t}$, the unsupervised domain adaptation for semantic segmentation is formulated as:

$$\begin{aligned} \theta^* &= \arg \min_{\theta} \sum_{i,j} [\mathcal{L}_s(F(\mathbf{x}_s^i, \theta), \hat{\mathbf{y}}_s^i) + \mathcal{L}_t(F(\mathbf{x}_t^j, \theta))] \\ &= \arg \min_{\theta} \left[\mathbb{E}_{\mathbf{x}_s \sim p(\mathbf{x}_s), \hat{\mathbf{y}}_s \sim p(\hat{\mathbf{y}}_s)} [\mathcal{L}_s(F(\mathbf{x}_s, \theta), \hat{\mathbf{y}}_s)] \right. \\ &\quad \left. + \mathbb{E}_{\mathbf{x}_t \sim p(\mathbf{x}_t)} [\mathcal{L}_t(F(\mathbf{x}_t, \theta))] \right] \quad (1) \\ &= \arg \min_{\theta} \left[\mathbb{E}_{\mathbf{y}_s \sim p(\mathbf{y}_s), \hat{\mathbf{y}}_s \sim p(\hat{\mathbf{y}}_s)} [\mathcal{L}_s(\mathbf{y}_s, \hat{\mathbf{y}}_s)] \right. \\ &\quad \left. + \mathbb{E}_{\mathbf{y}_t \sim p(\mathbf{y}_t)} [\mathcal{L}_t(\mathbf{y}_t)] \right] \end{aligned}$$

where θ is the parameters of F , $p(\cdot)$ is the probability density function. As the labels for \mathcal{D}_s are available, \mathcal{L}_s can be

efficiently formulated as a supervised cross-entropy loss:

$$\mathcal{L}_s(\mathbf{y}_s, \hat{\mathbf{y}}_s) = - \sum_{h,w,c} \hat{\mathbf{y}}_s^{h,w,c} \log (\mathbf{y}_s^{h,w,c}) \quad (2)$$

where $\mathbf{y}^{h,w,c}$ and $\hat{\mathbf{y}}^{h,w,c}$ represent the predicted and ground-truth probabilities of the pixel at the location of (h, w) taking the label of c , respectively. Meanwhile, \mathcal{L}_t handles unlabeled data from the target domain where the ground-truth labels are not available. To alleviate this label lacking issue, several forms of $\mathcal{L}_t(\mathbf{y}_t)$ have been exploited such as cross-entropy loss with pseudo-labels [20], Probability Distribution Divergence (i.e. Adversarial loss defined via an additional Discriminator) [6], [7], or entropy formulation [8], [22].

Entropy minimization revisited. By adopting the Shannon entropy formulation to the target prediction and constraining function F to produce a high-confident prediction, \mathcal{L}_t can be formulated as

$$\mathcal{L}_t(\mathbf{y}_t) = \frac{-1}{\log(C)} \sum_{h,w,c} \mathbf{y}_t^{h,w,c} \log (\mathbf{y}_t^{h,w,c}). \quad (3)$$

Although this form of \mathcal{L}_t can give a direct assessment of the predicted segmentation maps, it tends to be dominated by the high probability areas (since the high probability areas produce a higher value updated gradient due to $\lim_{\mathbf{y}_t^{h,w,c} \rightarrow 1} \frac{-\partial \mathcal{L}_t(\mathbf{y}_t)}{\partial \mathbf{y}_t^{h,w,c}} = \frac{1}{\log(C)}$ and $\lim_{\mathbf{y}_t^{h,w,c} \rightarrow 0} \frac{-\partial \mathcal{L}_t(\mathbf{y}_t)}{\partial \mathbf{y}_t^{h,w,c}} = -\infty$), i.e. easy classes, rather than difficult classes [8]. More importantly, this is essentially a pixel-wise formation, where pixels are treated independently of each other. Consequently, the structural information is usually neglected in this form. This issue could lead to a confusion point during training process where two predicted segmentation maps have similar entropy but different segmentation accuracy, one correct and other incorrect as shown in Fig 3.

A. Unaligned Domain Scores (UDS)

In the entropy formulation, the pixel independent constraints are employed to convert the image-level metric to pixel-level metric. In contrast, we propose an image-level UDS metric that can directly evaluate the structural quality of \mathbf{y}_t . Particularly,

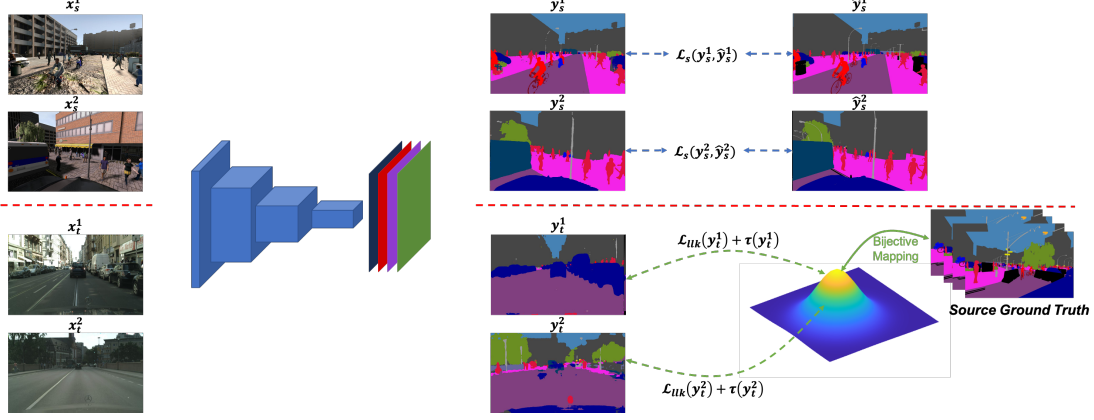


Fig. 4. **The Proposed BiMaL Framework.** The RGB image input is firstly forwarded to a deep semantic segmentation network to produce a segmentation map. The supervised loss is employed on the source training samples. Meanwhile, the predicted segmentation on target training samples will be mapped to the latent space to compute the Bijective Maximum Likelihood loss. The bijective mapping network is trained on the ground-truth images of the source domain.

let $p_t(\mathbf{y}_t)$ and $q_t(\mathbf{y}_t)$ be the probability mass functions of the predicted distribution and the real (actual) distribution of the predicted segmentation map \mathbf{y}_t , respectively. UDS metric measuring the efficiency of function G on the target dataset can be expressed as follows:

$$\text{UDS} = \mathbb{E}_{\mathbf{y}_t \sim p(\mathbf{y}_t)} \mathcal{L}_Y(p_t(\mathbf{y}_t), q_t(\mathbf{y}_t)) = \int \mathcal{L}_Y(p_t(\mathbf{y}_t), q_t(\mathbf{y}_t)) p_t(\mathbf{y}_t) d\mathbf{y}_t, \quad (4)$$

where $\mathcal{L}_Y(p_t(\mathbf{y}_t), q_t(\mathbf{y}_t))$ defines the distance between two distributions $p_t(\mathbf{y}_t)$ and $q_t(\mathbf{y}_t)$. Since there is no label for sample in the target domain, the direct access to $q_t(\mathbf{y}_t)$ is not available. Note that although \mathbf{x}_s and \mathbf{x}_t could vary significantly in image space (e.g. difference in pixel appearance due to lighting, scenes, weather), their segmentation maps \mathbf{y}_t and \mathbf{y}_s share similar distributions in terms of both class distributions as well as global and local structural constraints (sky has to be above roads, trees should be on sidewalks, vehicles should be on roads, etc.). Therefore, one can practically adopted the prior knowledge learned from segmentation labels of the source domains for $q_t(\mathbf{y}_t)$ as

$$\text{UDS} \approx \int \mathcal{L}_Y(p_t(\mathbf{y}_t), q_s(\mathbf{y}_t)) p_t(\mathbf{y}_t) d\mathbf{y}_t, \quad (5)$$

where the distribution $q_s(\mathbf{y}_t)$ is the probability mass functions of the real distribution learned from ground-truth segmentation maps of \mathcal{D}_s . As a result, the proposed UDS metric can be computed without the requirement of labeled target data for learning the density of segmentation maps in target domain. There are several choices for \mathcal{L}_Y to estimate the divergence between the two distributions $p_t(\mathbf{y}_t)$ and $q_s(\mathbf{y}_t)$. In this paper, we adopt the common metric such as Kullback–Leibler (KL) formula for \mathcal{L}_Y . Note that other metrics are also applicable in the proposed UDS formulation. Moreover, to enhance the smoothness of the predicted semantic segmentation, a regularization term τ is imposed into \mathcal{L}_Y as

$$\mathcal{L}_Y(p_t(\mathbf{y}_t), q_s(\mathbf{y}_t)) = \log\left(\frac{p_t(\mathbf{y}_t)}{q_s(\mathbf{y}_t)}\right) + \tau(\mathbf{y}_t). \quad (6)$$

By computing UDS, one can measure the quality of the predicted segmentation maps \mathbf{y}_t on the target data.

In the next sections, we firstly discuss in details the learning process of $q_s(\mathbf{y}_t)$, and then derivations of the UDS metric for the novel Bijective Maximum Likelihood loss.

B. Learning Distribution with Bijective Mapping on the Source Domain

Let $G : \mathcal{Y} \rightarrow \mathcal{Z}$ be the bijective mapping function that maps a segmentation $\hat{\mathbf{y}}_s \in \mathcal{Y}$ to the latent space \mathcal{Z} , i.e. $\hat{\mathbf{z}}_s = G(\hat{\mathbf{y}}_s, \theta_F)$, where $\hat{\mathbf{z}}_s \sim q_z(\hat{\mathbf{z}}_s)$ is the latent variable, and q_z is the prior distribution. Then, the probability distribution $q_s(\hat{\mathbf{y}}_s)$ can be formulated via the change of variable formula:

$$\log(q_s(\hat{\mathbf{y}}_s)) = \log(q_z(\hat{\mathbf{z}}_s)) + \log\left(\left|\frac{\partial G(\hat{\mathbf{y}}_s, \theta_G)}{\partial \hat{\mathbf{y}}_s}\right|\right), \quad (7)$$

where θ_F is the parameters of G , $\left|\frac{\partial G(\hat{\mathbf{y}}_s, \theta_G)}{\partial \hat{\mathbf{y}}_s}\right|$ denotes the Jacobian determinant of function $G(\hat{\mathbf{y}}_s, \theta_G)$ with respect to $\hat{\mathbf{y}}_s$. To learn the mapping function, the negative log-likelihood will be minimized as follows:

$$\begin{aligned} \theta_G^* &= \arg \min_{\theta_G} \mathbb{E}_{\hat{\mathbf{y}}_s \sim q_s(\hat{\mathbf{y}}_s)} \left[-\log(q_s(\hat{\mathbf{y}}_s)) \right] \\ &= \arg \min_{\theta_G} \mathbb{E}_{\hat{\mathbf{z}}_s \sim q_z(\hat{\mathbf{z}}_s)} \left[-\log(q_z(\hat{\mathbf{z}}_s)) - \log\left(\left|\frac{\partial G(\hat{\mathbf{y}}_s, \theta_G)}{\partial \hat{\mathbf{y}}_s}\right|\right) \right]. \end{aligned} \quad (8)$$

In general, there are various choices for the prior distribution q_z . However, the ideal distribution should satisfy two criteria: (1) simplicity in the density estimation, and (2) easy in sampling. Considering the two criteria, we choose Normal distribution as the prior distribution q_z . Note that any other distribution is also feasible as long as it satisfies the mentioned criteria.

To enforce the information flow from a segmentation domain to a latent space with different abstraction levels, the bijective function G can be further formulated as a composition of several sub-bijective functions g_i as $G = g_1 \circ g_2 \circ \dots \circ g_K$, where K is the number of sub-functions. The Jacobian $\frac{\partial G}{\partial \hat{\mathbf{y}}_s}$ can be derived by $\frac{\partial G}{\partial \hat{\mathbf{y}}_s} = \frac{\partial g_1}{\partial \hat{\mathbf{y}}_s} \cdot \frac{\partial g_2}{\partial f_1} \dots \frac{\partial g_K}{\partial f_{K-1}}$. With this structure, the properties of each g_i will define the properties for the whole bijective mapping function G . Interestingly, with this form, G becomes a DNN structure when g_i is a non-linear function built from a composition of convolutional layers. Several DNN structures [52]–[58] can be adopted for sub-functions.

C. Bijective Maximum Likelihood (BiMaL) Loss

In this section, we present the proposed Bijective Maximum Likelihood (BiMaL) which can be used as the loss of target domain \mathcal{L}_t .

1) *BiMaL formulation*: From Eqns. (5) and (6), UDS metric can be rewritten as follows:

$$\begin{aligned} \text{UDS} &= \int \left[\log \left(\frac{p_t(\mathbf{y}_t)}{q_s(\mathbf{y}_t)} \right) + \tau(\mathbf{y}_t) \right] p_t(\mathbf{y}_t) d\mathbf{y}_t \\ &= \mathbb{E}_{\mathbf{y}_t \sim p_t(\mathbf{y}_t)} [\log(p_t(\mathbf{y}_t))] \\ &\quad - \mathbb{E}_{\mathbf{y}_t \sim p_t(\mathbf{y}_t)} [\log(q_s(\mathbf{y}_t))] + \mathbb{E}_{\mathbf{y}_t \sim p_t(\mathbf{y}_t)} [\tau(\mathbf{y}_t)] \\ &\leq \mathbb{E}_{\mathbf{y}_t \sim p_t(\mathbf{y}_t)} [-\log(q_s(\mathbf{y}_t)) + \tau(\mathbf{y}_t)] \end{aligned} \quad (9)$$

It should be noticed that with any form of the distribution p_t , the above inequality still holds as $p_t(\mathbf{y}_t) \in [0, 1]$ and $\log(p_t(\mathbf{y}_t)) \leq 0$. Now, we define our Bijective Maximum Likelihood Loss as

$$\mathcal{L}_t(\mathbf{y}_t) = -\log(q_s(\mathbf{y}_t)) + \tau(\mathbf{y}_t), \quad (10)$$

where $\log(q_s(\mathbf{y}_t))$ defines the log-likelihood of \mathbf{y}_t with respect to the density function q_s . Then, by adopting the bijective function G learned from Eqn. (8) using samples from source domain and the prior distribution q_z , the first term of $\mathcal{L}_t(\mathbf{y}_t)$ in Eqn. (10) can be efficiently computed via log-likelihood formulation:

$$\begin{aligned} \mathcal{L}_{llk}(\mathbf{y}_t) &= -\log(q_s(\mathbf{y}_t)) \\ &= -\log(q_z(\mathbf{z}_t)) - \log \left(\left| \frac{\partial G(\mathbf{y}_t, \theta_G)}{\partial \mathbf{y}_t} \right| \right), \end{aligned} \quad (11)$$

where $\mathbf{z}_t = G(\mathbf{y}_t, \theta_G)$. Thanks to the bijective property of the mapping function G , the minimum negative log-likelihood loss $\mathcal{L}_{llk}(\mathbf{y}_t)$ can be effectively computed via the density of the prior distribution q_z and its associated Jacobian determinant $\left| \frac{\partial G(\mathbf{y}_t, \theta_G)}{\partial \mathbf{y}_t} \right|$. For the second term of $\mathcal{L}_t(\mathbf{y}_t)$, we further enhance the smoothness of the predicted semantic segmentation with the pair-wised formulation to encourage similar predictions for neighbourhood pixels with similar color:

$$\tau(\mathbf{y}_t) = \sum_{h,w} \sum_{h',w'} \exp \left\{ -\frac{\|\mathbf{x}_t^{h,w} - \mathbf{x}_t^{h',w'}\|_2^2}{2\sigma_1^2} - \frac{\|\mathbf{y}_t^{h,w} - \mathbf{y}_t^{h',w'}\|_2^2}{2\sigma_2^2} \right\} \quad (12)$$

where $(h', w') \in \mathcal{N}_{h,w}$ denotes the neighbourhood pixels of (h, w) , $\mathbf{x}^{h,w}$ represents the color at pixel (h, w) ; and $\{\sigma_1, \sigma_2\}$ are the hyper parameters controlling the scale of Gaussian kernels. It should be noted that any regularizers [1], [59] enhancing the smoothness of the segmentation results can also be adopted for τ . Putting Eqns. (10), (11), (12) to Eqn (1), the objective function can be rewritten as:

$$\begin{aligned} \theta^* &= \arg \min_{\theta} \left[\mathbb{E}_{\mathbf{y}_s \sim p(\mathbf{y}_s), \hat{\mathbf{y}}_s \sim p(\hat{\mathbf{y}}_s)} [\mathcal{L}_s(\mathbf{y}_s, \hat{\mathbf{y}}_s)] \right. \\ &\quad \left. + \mathbb{E}_{\mathbf{y}_t \sim p(\mathbf{y}_t)} [\mathcal{L}_{llk}(\mathbf{y}_t) + \tau(\mathbf{y}_t)] \right] \end{aligned} \quad (13)$$

Figure 4 illustrates our proposed BiMaL framework to learn the deep segmentation network G . Also, we can prove that direct entropy minimization as Eqn. (3) is just a particular case of our log likelihood maximization. We will further discuss how our maximum likelihood can cover the case of pixel-independent entropy minimization in Section III-C3.

2) *BiMaL properties: Global Structure Learning*. Sharing similar property with [54], [55], [60]–[62], from Eqn. (7), as the learned density function is adopted for the entire segmentation map $\hat{\mathbf{y}}_s$, the global structure in $\hat{\mathbf{y}}_s$ can be efficiently captured and modeled.

Tractability and Invertibility. Thanks to the designed bijection F , the complex distribution of segmentation maps can be efficiently captured. Moreover, the mapping function is bijective, and, therefore, both inference and generation are exact and tractable.

3) *Relation to Entropy Minimization*: The first term of UDS in Eqn. (9) can be derived as

$$\begin{aligned} \int \log \left(\frac{p_t(\mathbf{y})}{q_s(\mathbf{y})} \right) p_t(\mathbf{y}) d\mathbf{y}_t &\geq 0 \\ \Leftrightarrow \mathbb{E}_{\mathbf{y}_t \sim p_t(\mathbf{y}_t)} [\log(p_t(\mathbf{y}_t)) - \log(q_s(\mathbf{y}_t))] &\geq 0 \\ \Leftrightarrow \mathbb{E}_{\mathbf{y}_t \sim p_t(\mathbf{y}_t)} [-\log(q_s(\mathbf{y}_t))] &\geq \mathbb{E}_{\mathbf{y}_t \sim p_t(\mathbf{y}_t)} [-\log(p_t(\mathbf{y}_t))] \\ \Leftrightarrow \mathbb{E}_{\mathbf{y}_t \sim p_t(\mathbf{y}_t)} [\mathcal{L}_{llk}(\mathbf{y}_t)] &\geq \text{Ent}(\mathbf{Y}_t) \end{aligned} \quad (14)$$

where \mathbf{Y}_t is the random variable with possible values $\mathbf{y}_t \sim p_t(\mathbf{y}_t)$, and $\text{Ent}(\mathbf{Y}_t)$ denotes the entropy of the random variable \mathbf{Y}_t . It can be seen that the proposed negative log-likelihood \mathcal{L}_{llk} is an upper bound of the entropy of \mathbf{Y}_t . Therefore, minimizing our proposed BiMaL loss will also enforce the entropy minimization process. Moreover, by not assuming pixel independence, our proposed BiMaL can model and evaluate structural information at the image-level better than previous pixel-level approaches [8], [22], [27].

IV. CROSS-DOMAIN LONG-TAIL ADAPTATION FOR SEMANTIC SEGMENTATION

As shown in Fig. 2, in Semantic Segmentation task, there is another challenging issue that can significantly affect the performance of domain adaptation approaches, i.e. the long-tail issue. This occurs in both labeled source domain **and** new **unlabeled** target domains. Unlike prior works where only labeled part is on their focus to alleviate the long-tail problem, our motivation is to address this issue in **both two domains** which is novel and more challenging. In this section, we further investigate the long-tail issue for adaptation in semantic segmentation. Then, a novel Conditional Maximum Likelihood (CoMaL) loss is further introduced to address the long-tail problem. Similar to BiMaL loss, the assumptions of pixel independence made by prior semantic segmentation methods are relaxed while more structural dependencies are efficiently taken into account during learning process.

A. Long-tail Problem in Domain Adaptation

Different from classification problem where a single class is predicted for each input sample/image, in semantic segmentation, \mathbf{y}_s and \mathbf{y}_t are segmentation maps whose each pixel has its own predicted class. Let $N = H \times W$ be the total number of pixels in an input image where H and W are the height and width of that image. In addition, let y_s^i (or y_t^i) be the predicted class of the i^{th} pixel in \mathbf{y}_s (or \mathbf{y}_t). Eqn. (1) can be rewritten as follows.

$$\begin{aligned}\theta^* &= \arg \min_{\theta} \left[\int \mathcal{L}_s(\mathbf{y}_s, \hat{\mathbf{y}}_s) q_s(\mathbf{y}_s) q_s(\hat{\mathbf{y}}_s) d\mathbf{y}_s d\hat{\mathbf{y}}_s + \int \mathcal{L}_t(\mathbf{y}_t) p_t(\mathbf{y}_t) d\mathbf{y}_t \right] \\ &= \arg \min_{\theta} \left[\int \sum_{i=1}^N \mathcal{L}_s(y_s^i, \hat{y}_s^i) q_s(y_s^i) q_s(y_s^i | y_s^i) q_s(\hat{y}_s^i) d\mathbf{y}_s d\hat{\mathbf{y}}_s \right. \\ &\quad \left. + \int \sum_{i=1}^N \mathcal{L}_t(y_t^i) p_t(y_t^i) p_t(y_t^i | y_t^i) d\mathbf{y}_t \right] \quad (15)\end{aligned}$$

where \mathbf{y}_s^i (or \mathbf{y}_t^i) is a predicted segmentation map conditional on the prediction of the i^{th} pixel; $q_s(y_s^i)$ and $p_t(y_t^i)$ are the class distributions received by a pixel of the data, $q_s(\mathbf{y}_s^i | y_s^i)$ and $p_t(\mathbf{y}_t^i | y_t^i)$ represent the conditional structure constraints of the segmentation. From Eqn. (15), two main properties are required to be addressed during optimization process, i.e. (1) *long-tail problem* and (2) *structural learning* for semantic segmentation.

Long-tail Problem. In practice, the class distributions $q_s(y_s^i)$ and $p_t(y_t^i)$ in both source and target domains suffer heavy long-tail problems as illustrated in Fig. 2. As the learning gradient is updated based on predicted class of each pixel, there is a bias toward the class occupying large regions. In other words, the gradients from pixels of the head classes (i.e. road, sky, sidewalk, cars) are largely dominant over the tail classes (i.e. poles, fences, or pedestrians) in an image. For example, let the segmentation image have only two classes where $q_s(y_s^i = 0) \ll q_s(y_s^i = 1)$, $N = N_0 + N_1$ where N_0 and N_1 are the number of pixels of class 0 and class 1, respectively. In addition, when the number of pixels of class 1 largely dominants class 0, i.e. $N_0 \ll N_1$, an inequality can be derived as follows.

$$\begin{aligned}\left\| \frac{\partial \int \sum_{i=1}^N \mathcal{L}_s(y_s^i, \hat{y}_s^i) q_s(y_s^i) q_s(y_s^i | y_s^i) q_s(\hat{y}_s^i) d\mathbf{y}_s d\hat{\mathbf{y}}_s}{\partial \mathbf{y}_s^{(0)}} \right\| &\ll \\ \left\| \frac{\partial \int \sum_{i=1}^N \mathcal{L}_s(y_s^i, \hat{y}_s^i) q_s(y_s^i) q_s(y_s^i | y_s^i) q_s(\hat{y}_s^i) d\mathbf{y}_s d\hat{\mathbf{y}}_s}{\partial \mathbf{y}_s^{(1)}} \right\| &\quad (16)\end{aligned}$$

where $\|\cdot\|$ is the magnitude of the vector, $\mathbf{y}_s^{(0)}$ (or $\mathbf{y}_s^{(1)}$) represent the predicted probabilities of label 0 (or 1). As shown in Eqn. (16), when the distribution of class 1 largely dominants class 0, the losses defined in the source domain incline to produce large gradient updates for the head classes; meanwhile, the gradients of tail classes tend to be suppressed. A similar observation is also made in [24]. Similar to the source domain, this long-tail problem also occurs in the target domain.

Structural Learning for Semantic Segmentation in Source and Target domain. In Eqn. (15), one can see that both terms of $q_s(\mathbf{y}_s^i | y_s^i)$ and $p_t(\mathbf{y}_t^i | y_t^i)$ reflect the dependencies of pixels in their predictions. In prior works which focus only on learning semantic segmentation on source domain (i.e. where labels are available), supervised loss can help to partially and implicitly maintain the structure in \mathbf{y}_s . However, as labels are not available in the target domain, pixel independence is usually assumed for \mathcal{L}_t [8], [18], [19], [22] to be applicable. Then, only a weak indication of structural learning via Adversarial loss is adopted.

In the next sections, we first propose a novel metric that addresses both properties in its formulation. Then its derivation

as well as the conditional structural learning of $q_s(\mathbf{y}_s^i | y_s^i)$ and $p_t(\mathbf{y}_t^i | y_t^i)$ are presented for the learning process.

B. Learning Segmentation From Distributions with Conditional Maximum Likelihood (CoMaL) loss

As in Section IV-A, the long-tail issues occur in semantic segmentation due to the imbalance in class distributions, where the densities of head classes dominates those of the tail classes. Therefore, rather than directly deriving the formulation of Eqn. (15) with the given training data distribution, we first assume a presence of an ideal dataset whose classes are uniformly distributed. Then, based on this ideal distribution, the derivation are obtained for all terms in Eqn. (15). Finally, the presence of the ideal data is removed for the training procedure to be applicable in practise. By this way, the long-tail issue can be efficiently addressed and practically adopted for a given training data.

Formally, let $q'_s(\mathbf{y}_s), q'_s(\hat{\mathbf{y}}_s)$ be the ideal distributions of \mathbf{y}_s and $\hat{\mathbf{y}}_s$ in source domain, and $p'_t(\mathbf{y}_t)$ represent the ideal distribution of the target domain. By learning from these ideal distributions, the numbers of pixels across classes in both domains become more balanced, and, therefore, alleviating the long-tail problem of semantic segmentation in predictions of both source and target domains. Learning an SDA model with respect to $q'_s(\mathbf{y}_s), q'_s(\hat{\mathbf{y}}_s)$ and $p'_t(\mathbf{y}_t)$ can be adopted to Eqn. (15) as follows.

$$\begin{aligned}\theta^* &= \arg \min_{\theta} \left[\int \mathcal{L}_s(\mathbf{y}_s, \hat{\mathbf{y}}_s) q'_s(\mathbf{y}_s) q'_s(\hat{\mathbf{y}}_s) d\mathbf{y}_s d\hat{\mathbf{y}}_s + \int \mathcal{L}_t(\mathbf{y}_t) p'_t(\mathbf{y}_t) d\mathbf{y}_t \right] \\ &= \arg \min_{\theta} \left[\mathbb{E}_{\mathbf{y}_s \sim q_s(\mathbf{y}_s), \hat{\mathbf{y}}_s \sim q_s(\hat{\mathbf{y}}_s)} \mathcal{L}_s(\mathbf{y}_s, \hat{\mathbf{y}}_s) \frac{q'_s(\mathbf{y}_s) q'_s(\hat{\mathbf{y}}_s)}{q_s(\mathbf{y}_s) q_s(\hat{\mathbf{y}}_s)} \right. \\ &\quad \left. + \mathbb{E}_{\mathbf{y}_t \sim p_t(\mathbf{y}_t)} \mathcal{L}_t(\mathbf{y}_t) \frac{p'_t(\mathbf{y}_t)}{p_t(\mathbf{y}_t)} \right] \quad (17)\end{aligned}$$

The fractions between the ideal distributions and data distributions, i.e. $\frac{q'_s(\mathbf{y}_s) q'_s(\hat{\mathbf{y}}_s)}{q_s(\mathbf{y}_s) q_s(\hat{\mathbf{y}}_s)}$ and $\frac{p'_t(\mathbf{y}_t)}{p_t(\mathbf{y}_t)}$, can be interpreted as the complement of the long-tail distributions to improve the class balanced during learning process, and, hence, enhance the robustness of the learned segmentation model against long-tail data.

It is noticed that, the fraction between the ideal distribution $q'_s(\hat{\mathbf{y}}_s)$ and the long-tailed distribution $q_s(\hat{\mathbf{y}}_s)$ is a constant as these are the distributions over the ground truths. Therefore, it can be efficiently ignored during the optimization process. Eqn. (17) can be rewritten as follows:

$$\begin{aligned}\theta^* &= \arg \min_{\theta} \left[\mathbb{E}_{\mathbf{y}_s \sim q_s(\mathbf{y}_s), \hat{\mathbf{y}}_s \sim q_s(\hat{\mathbf{y}}_s)} \mathcal{L}_s(\mathbf{y}_s, \hat{\mathbf{y}}_s) \frac{q'_s(\mathbf{y}_s)}{q_s(\mathbf{y}_s)} \right. \\ &\quad \left. + \mathbb{E}_{\mathbf{y}_t \sim p_t(\mathbf{y}_t)} \mathcal{L}_t(\mathbf{y}_t) \frac{p'_t(\mathbf{y}_t)}{p_t(\mathbf{y}_t)} \right] \\ &= \arg \min_{\theta} \left[\mathbb{E}_{\mathbf{y}_s \sim q_s(\mathbf{y}_s), \hat{\mathbf{y}}_s \sim q_s(\hat{\mathbf{y}}_s)} \sum_{i=1}^N \mathcal{L}_s(y_s^i, \hat{y}_s^i) \frac{q'_s(y_s^i) q'_s(y_s^i | y_s^i)}{q_s(y_s^i) q_s(y_s^i | y_s^i)} \right. \\ &\quad \left. + \mathbb{E}_{\mathbf{y}_t \sim p_t(\mathbf{y}_t)} \sum_{i=1}^N \mathcal{L}_t(y_t^i) \frac{p'_t(y_t^i) p'_t(y_t^i | y_t^i)}{p_t(y_t^i) p_t(y_t^i | y_t^i)} \right] \quad (18)\end{aligned}$$

Notice that as the labels of samples in this domain are not accessible, a direct computation of distributions in the target

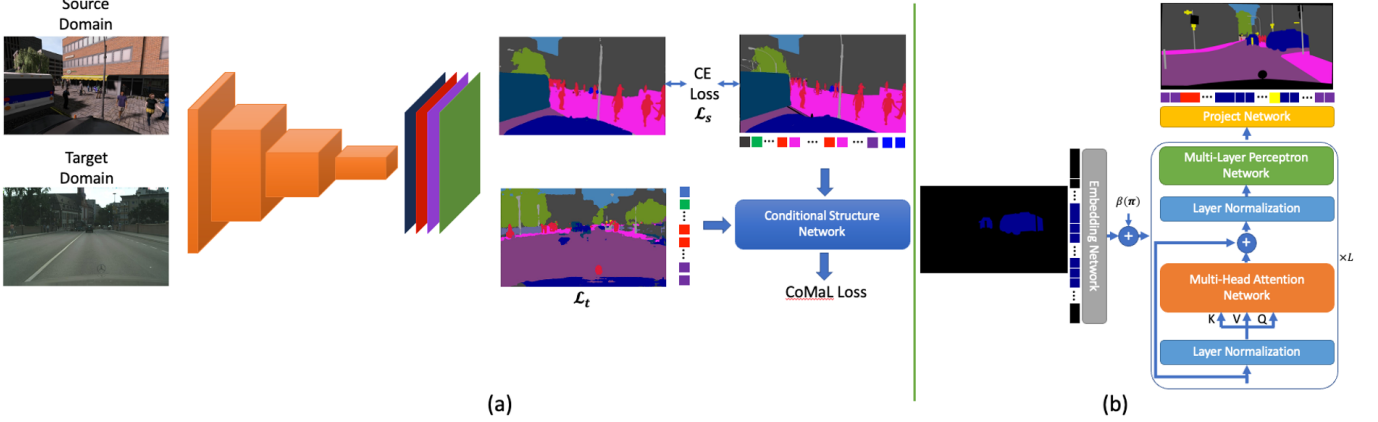


Fig. 5. **The Proposed Framework.** (a) The Self-supervised Adaptation Framework. The cross-entropy (CE) loss (\mathcal{L}_s) is applied on the source domain and the target loss \mathcal{L}_t is deployed on the target domains. The segmentation on both domains are forwarded into the Conditional Structure Network to compute the Conditional Maximum Likelihood (CoMaL) loss. (b) The Conditional Structure Network.

domain, i.e. $p_t(\mathbf{y}_t)$ and $p'_t(\mathbf{y}_t)$, is not feasible. Generally, one can see that although input images of source domain (\mathbf{x}_s) and target domain (\mathbf{x}_t) could vary significantly in the image space according to their differences in pixel appearance across domains (such as lighting, scenes, weather, etc.), their segmentation maps \mathbf{y}_s and \mathbf{y}_t share similar class distributions as well as global and local structure (sky has to be above roads, trees should be on side-walks, vehicles should be on roads, etc.). Therefore, the prior knowledge of segmentation maps $q_s(\mathbf{y}_s)$ and $q'_s(\mathbf{y}_s)$ can be practically adopted for $p_t(\mathbf{y}_t)$ and $p'_t(\mathbf{y}_t)$, respectively. As a result, Eqn. (18) can be rewritten as follows:

$$\theta^* = \arg \min_{\theta} \left[\mathbb{E}_{\mathbf{y}_s \sim q_s(\mathbf{y}_s), \hat{\mathbf{y}}_s \sim q_s(\hat{\mathbf{y}}_s)} \sum_{i=1}^N \mathcal{L}_s(\mathbf{y}_s^i, \hat{\mathbf{y}}_s^i) \frac{q'_s(\mathbf{y}_s^i) q'_s(\mathbf{y}_s^i | \mathbf{y}_s^i)}{q_s(\mathbf{y}_s^i) q_s(\mathbf{y}_s^i | \mathbf{y}_s^i)} \right. \\ \left. + \mathbb{E}_{\mathbf{y} \sim q_s(\mathbf{y}_t)} \sum_{i=1}^N \mathcal{L}_t(\mathbf{y}_t^i) \frac{q'_s(\mathbf{y}_t^i) q'_s(\mathbf{y}_t^i | \mathbf{y}_t^i)}{q_s(\mathbf{y}_t^i) q_s(\mathbf{y}_t^i | \mathbf{y}_t^i)} \right] \quad (19)$$

By taking the logarithm of Eqn (19), a new objective function can be derived as follows (the full proof of Eqn. (20) will be available in the supplementary material):

$$\theta^* \simeq \arg \min_{\theta} \left[\mathbb{E}_{\mathbf{y}_s \sim q_s(\mathbf{y}_s), \hat{\mathbf{y}}_s \sim q_s(\hat{\mathbf{y}}_s)} \mathcal{L}_s(\mathbf{y}_s, \hat{\mathbf{y}}_s) + \mathbb{E}_{\mathbf{y} \sim q_s(\mathbf{y}_t)} \mathcal{L}_t(\mathbf{y}_t) \right. \\ \left. + \frac{1}{N} \sum_{i=1}^N \left(\mathbb{E}_{\mathbf{y}_s \sim q_s(\mathbf{y}_s), \hat{\mathbf{y}}_s \sim q_s(\hat{\mathbf{y}}_s)} \log \left(\frac{q'_s(\mathbf{y}_s^i)}{q_s(\mathbf{y}_s^i)} \right) \right. \right. \\ \left. \left. + \mathbb{E}_{\mathbf{y} \sim q_s(\mathbf{y}_t)} \log \left(\frac{q'_s(\mathbf{y}_t^i)}{q_s(\mathbf{y}_t^i)} \right) \right) \right] \quad (20)$$

$$+ \frac{1}{N} \sum_{i=1}^N \left(\mathbb{E}_{\mathbf{y}_s \sim q_s(\mathbf{y}_s), \hat{\mathbf{y}}_s \sim q_s(\hat{\mathbf{y}}_s)} \log \left(\frac{q'_s(\mathbf{y}_s^i | \mathbf{y}_s^i)}{q_s(\mathbf{y}_s^i | \mathbf{y}_s^i)} \right) \right. \\ \left. + \mathbb{E}_{\mathbf{y} \sim q_s(\mathbf{y}_t)} \log \left(\frac{q'_s(\mathbf{y}_t^i | \mathbf{y}_t^i)}{q_s(\mathbf{y}_t^i | \mathbf{y}_t^i)} \right) \right) \right]$$

From Eqn. (20), several constraints are introduced for the learning process.

Base Terms For Domain Adaptation. The first two terms of \mathcal{L}_s and \mathcal{L}_t are the supervised and self-supervised terms which help to embed the knowledge of labeled samples from source domain $\{\mathcal{X}_s, \mathcal{Y}_s\}$ and unlabeled samples of target domain $\{\mathcal{X}_t\}$.

Class-Balanced Learning. The next two terms $\log \left(\frac{q'_s(\mathbf{y}_s^i)}{q_s(\mathbf{y}_s^i)} \right)$ and $\log \left(\frac{q'_s(\mathbf{y}_t^i)}{q_s(\mathbf{y}_t^i)} \right)$ can be computed from the training dataset during learning procedure. Notice that since $q'_s(\mathbf{y}_s^i)$ is a uniform distribution, its likelihood is a constant number. Therefore, this term can be efficiently ignored during learning process. Let us denote these fractions as the class-weighted loss \mathcal{L}_{cls} , e.g. $\mathcal{L}_{cls}(y_s^i) = \log \left(\frac{q'_s(\mathbf{y}_s^i)}{q_s(\mathbf{y}_s^i)} \right)$.

Conditional Structural Learning. The last two terms $\log \left(\frac{q'_s(\mathbf{y}_s^i | \mathbf{y}_s^i)}{q_s(\mathbf{y}_s^i | \mathbf{y}_s^i)} \right)$ and $\log \left(\frac{q'_s(\mathbf{y}_t^i | \mathbf{y}_t^i)}{q_s(\mathbf{y}_t^i | \mathbf{y}_t^i)} \right)$ regularize the conditional structure of the segmentation. In practice, as the ideal dataset is not available, the direct access to the conditional distributions $q'_s(\mathbf{y}_s^i | \mathbf{y}_s^i)$ and $q'_s(\mathbf{y}_t^i | \mathbf{y}_t^i)$ is not feasible. Therefore, rather than directly computing these terms, they can be derived as follows.

$$\mathbb{E}_{\mathbf{y}_s \sim q_s(\mathbf{y}_s), \hat{\mathbf{y}}_s \sim q_s(\hat{\mathbf{y}}_s)} \log \left(\frac{q'_s(\mathbf{y}_s^i | \mathbf{y}_s^i)}{q_s(\mathbf{y}_s^i | \mathbf{y}_s^i)} \right) + \mathbb{E}_{\mathbf{y} \sim q_s(\mathbf{y}_t)} \log \left(\frac{q'_s(\mathbf{y}_t^i | \mathbf{y}_t^i)}{q_s(\mathbf{y}_t^i | \mathbf{y}_t^i)} \right) \\ = \mathbb{E}_{\mathbf{y}_s \sim q_s(\mathbf{y}_s), \hat{\mathbf{y}}_s \sim q_s(\hat{\mathbf{y}}_s)} \left[\log q'_s(\mathbf{y}_s^i | \mathbf{y}_s^i) - \log q_s(\mathbf{y}_s^i | \mathbf{y}_s^i) \right] \\ + \mathbb{E}_{\mathbf{y} \sim q_s(\mathbf{y}_t)} \left[\log q'_s(\mathbf{y}_t^i | \mathbf{y}_t^i) - \log q_s(\mathbf{y}_t^i | \mathbf{y}_t^i) \right] \quad (21)$$

$$\leq \mathbb{E}_{\mathbf{y}_s \sim q_s(\mathbf{y}_s), \hat{\mathbf{y}}_s \sim q_s(\hat{\mathbf{y}}_s)} \underbrace{- \log q_s(\mathbf{y}_s^i | \mathbf{y}_s^i)}_{\mathcal{L}_{CoMaL}(\mathbf{y}_s^i)} + \mathbb{E}_{\mathbf{y} \sim q_s(\mathbf{y}_t)} \underbrace{- \log q_s(\mathbf{y}_t^i | \mathbf{y}_t^i)}_{\mathcal{L}_{CoMaL}(\mathbf{y}_t^i)}$$

where \mathcal{L}_{CoMaL} is our proposed Conditional Maximum Likelihood loss. For any form of ideal distribution $q'_s(\cdot)$, our above inequality holds true as $q'_s(\cdot) \in [0, 1] \Leftrightarrow \log q'_s(\cdot) \leq 0$. Thanks to this inequality, the requirement of the ideal dataset can be effectively relaxed for the learning process.

As a result, the entire self-supervised domain adaptation in long-tail segmentation framework can be optimized as:

$$\theta^* = \arg \min_{\theta} \frac{1}{N} \left[\mathbb{E}_{\mathbf{y}_s \sim q_s(\mathbf{y}_s), \hat{\mathbf{y}}_s \sim q_s(\hat{\mathbf{y}}_s)} \left[\mathcal{L}_s(\mathbf{y}_s, \hat{\mathbf{y}}_s) \right. \right. \\ \left. \left. + \frac{1}{N} \sum_{i=1}^N \left(\mathcal{L}_{cls}(\hat{\mathbf{y}}_s^i) + \mathcal{L}_{CoMaL}(\hat{\mathbf{y}}_s^i) \right) \right] \right] \\ + \mathbb{E}_{\mathbf{y}_t \sim q_s(\mathbf{y}_t)} \left[\mathcal{L}_t(\mathbf{y}_t) + \frac{1}{N} \sum_{i=1}^N \left(\mathcal{L}_{cls}(\mathbf{y}_t^i) + \mathcal{L}_{CoMaL}(\mathbf{y}_t^i) \right) \right] \quad (22)$$

In our approach, the loss \mathcal{L}_t on the target domain is defined as the self-supervised loss with pseudo labels as [19]. Fig. 5(a)

illustrates our proposed framework. In the next section, we further discuss the learning process of the conditional structure $q_s(\mathbf{y}_s^i | \mathbf{y}_s^i)$ on the ground truth of the source domain.

C. The Conditional Structure Learning

Given the segmentation dataset of the source domain, $\mathbf{y}_s \in \mathcal{Y}_s$, the structural condition $q_s(\mathbf{y}_s^i | \mathbf{y}_s^i)$ can be auto-regressively modeled as follows:

$$\begin{aligned} \theta_G^* &= \arg \min_{\theta_G} -\mathbb{E}_{\mathbf{y}_s \sim \mathcal{Y}_s, \pi_i \in \Pi} [\log(q_s(\mathbf{y}_s^i | \mathbf{y}_s^i))] \\ &= \arg \min_{\theta_G} -\mathbb{E}_{\mathbf{y}_s \sim \mathcal{Y}_s, \pi_i \in \Pi} \sum_{j=2}^N \log(q_s(\mathbf{y}_s^j | \mathbf{y}_s^{\pi_1^i} \dots \mathbf{y}_s^{\pi_{j-1}^i}, \theta_G, \pi^i)) \end{aligned} \quad (23)$$

where π^i is a permutation of $\{1..N\}$ and $\pi_1^i = i$, θ_G is the parameters of the generative model G . The learning process can be solved by Recurrent Neural Networks (RNN) (i.e. PixelRNN, PixelCNN) [63]. However, a single model of PixelRNN (or PixelCNN) maintains a fixed permutation π , and the permutation's order π matters since it affects the structural constraints. Meanwhile, we need a different permutation π^i for each condition $q_s(\hat{\mathbf{y}}_s^i | \hat{\mathbf{y}}_s^i)$ according to the given conditional position on the segmentation. Therefore, straightforwardly adopting RNN-based models as in prior works for all possible different permutations π^i to compute $q_s(\mathbf{y}_s^i | \mathbf{y}_s^i)$ requires a burdensome training process with numerous models (i.e. one model for each permutation) which is infeasible.

Rather than learning numerous models for all possible orders π^i , we propose to represent \mathbf{y}_s as sequence of pixels and mask out the unknown pixels. Then, the model is trained to maximize the conditional density function of these unknown pixels given the known pixels. As a results, by varying the input masks, the model can effectively obtain the capability of learning the structure of the segmentation map \mathbf{y}_s given known pixels. Formally, let $\mathbf{m} \in \mathcal{M}$ be a binary mask where value of *one* indicates an unknown pixel and *zero* is a known pixel, so the problem of learning the structural condition can be formulated as follows:

$$\theta_G^* = -\arg \min_{\theta_G} \mathbb{E}_{\mathbf{y} \sim \mathcal{Y}, \mathbf{m} \sim \mathcal{M}} \log p(\mathbf{y}_s \odot \mathbf{m} | \mathbf{y}_s \odot (1 - \mathbf{m})) \quad (24)$$

where \odot denotes the Hadamard product, $\mathbf{m}^i = 1$ means that the pixel \mathbf{y}_s^i is the masked pixel and vice versa.

Eqn. (24) brings some interesting properties. *Firstly*, if the \mathbf{m} only contains one unmasked pixel, i.e., $\mathbf{m}^i = 0$ and $\forall j \in \{1..N\}, j \neq i : \mathbf{m}^j = 1$, the condition $p(\mathbf{y}_s \odot \mathbf{m} | \mathbf{y}_s \odot (1 - \mathbf{m}))$ is equivalent to $q_s(\mathbf{y}_s^i | \mathbf{y}_s^i)$. Under this condition, the network G can capture structural information of the segmentation conditioned on the given pixel. *Secondly*, if the binary mask only contains **1**, i.e. $\mathbf{m} = \mathbf{1}$, the condition $p(\mathbf{y}_s \odot \mathbf{m} | \mathbf{y}_s \odot (1 - \mathbf{m}))$ is equivalent to the likelihood of $p(\mathbf{y}_s)$. Then, the network learns the global structure and the spatial relationship among pixels. *Thirdly*, \mathbf{m} is not only limited to one unmasked pixel but also able to contain more than one unmasked pixel, it increases the flexibility of the model to learn the structures conditioned on the unmasked pixels.

To effectively learn the generative network G , we design it as a multi-head attention network, in which the spatial relationship and structure information can be learned by the attention

mechanism at the training time. Particularly, considering each single pixel as a separate token, we form the generator network G with L blocks of multihead attention network as follows:

$$\begin{aligned} \mathbf{z}_0 &= \alpha(\mathbf{y}_s \odot (1 - \mathbf{m})) + \beta(\boldsymbol{\pi}), \quad \mathbf{a}_l = \mathbf{z}_l + \gamma(\tau(\mathbf{z}_l)) \\ \mathbf{z}_{l+1} &= \mathbf{a}_l + \eta(\tau(\mathbf{a}_l)), \quad \bar{\mathbf{y}}_s = \phi(\tau(\mathbf{z}_L)) \end{aligned} \quad (25)$$

where $\tau(\cdot)$ is the normalization norm [64], $\alpha(\cdot)$ is the token embedding network, $\beta(\boldsymbol{\pi})$ is the learned positional embedding ($\boldsymbol{\pi} = [1, 2, \dots, N]$), $\gamma(\cdot)$ represents the multi-head attention layer, $\eta(\cdot)$ is the residual-style multi-layer perception network, and $\phi(\cdot)$ is the projection that maps the normalized output of the multi-attention network to the logits parameterizing the conditional distributions $p(\mathbf{y}_s \odot \mathbf{m} | \mathbf{y}_s \odot (1 - \mathbf{m}))$. The subscript l denotes the l^{th} block. Fig. 5(b) illustrates the structural condition network. To ensure the correct structural conditions, we apply the proper binary mask into the $N \times N$ attention matrix.

D. CoMaL properties

Global Structural Learning. Although these prior methods have achieved promising results for semantic segmentation, they usually adopted the pixel-independent assumption [19], [65] and addressed long-tailed issues by predefining class-balanced weights. However, as shown in Eqn. (18), under the assumption of pixel independence, the condition $\frac{q'_s(\mathbf{y}_s^i | \mathbf{y}_s^i)}{q_s(\mathbf{y}_s^i | \mathbf{y}_s^i)}$ has been ignored. This results in lacking of mechanisms for maintain the structural learning during training process. Meanwhile, the conditional structural learning is explicitly formulated in the objective function of Eqn. (18) and Section IV-C, our CoMaL approach has shown its advantages in capturing the global structure of \mathbf{y}_s and \mathbf{y}_t .

Class-balance Learning for both Source and Target Domains. Unlike prior works where only labeled part is on their focus, CoMaL framework addresses the *long-tail* issue in **both domains** which is novel and more challenging. Experiments in Table III (a,b) have emphasized the advantages of CoMaL on improving the semantic segmentation accuracy on new unlabeled domains.

Flexibility Learning without the need of an Ideal Dataset. CoMaL **does not require** the presence of ideal data in its training procedure. As in Eqn. (21), with any form of ideal distributions, the CoMaL loss is proven to be the upper bound of the loss obtained by ideal data. CoMaL also gives a flexibility in setting the desired class distribution $q'_s(\mathbf{y})$ even it is derived from non-uniform class distributions.

Relation to Markovian assumption. Rather than extracting neighborhood dependencies from local structures (i.e. pixels within a particular range) with Markovian assumption as in prior work, Eqn. (21), $q_s(\mathbf{y}_s^i | \mathbf{y}_s^i)$ emphasizes more on generalized structural constraints as it embeds dependencies on all remaining pixels of the segmentation map. Particularly, after learning the conditional distribution $q_s(\mathbf{y}_s^i | \mathbf{y}_s^i)$ via our proposed multihead attention network, during the training process, this term is considered as a metric to measure how good a predicted segmentation maintains the structural consistency (i.e., relative structure among objects) in comparison to the distributions of actual segmentation maps.

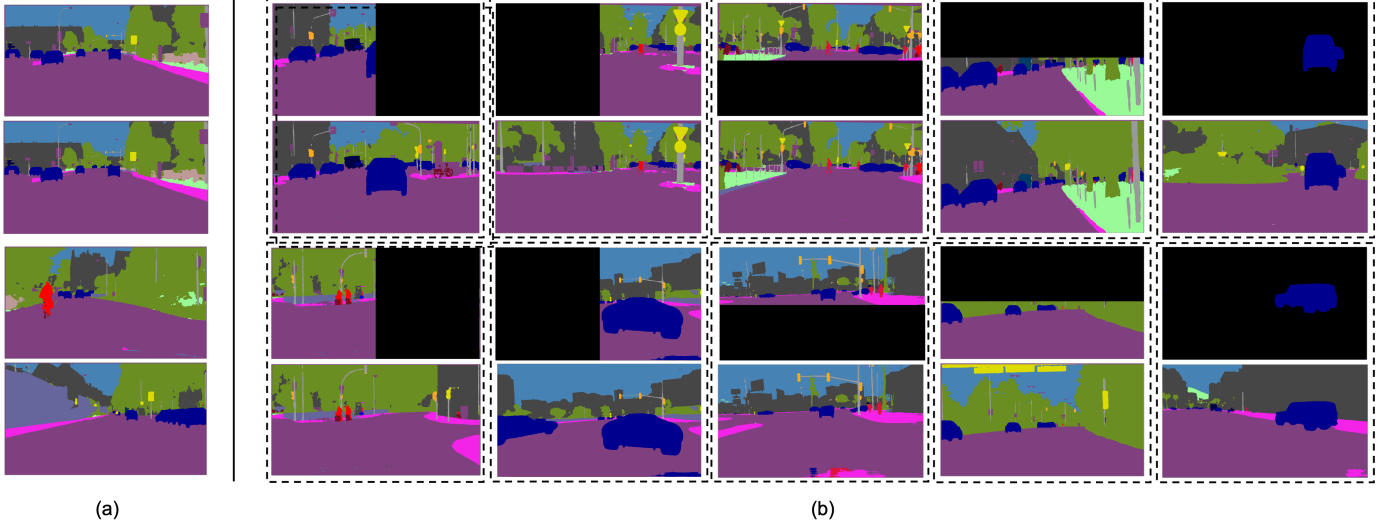


Fig. 6. Segmentation images sampled by the conditional structure network G . (a) Fully Sampled Images. (b) Sampled Images Conditioned on a Given Mask.

V. EXPERIMENTS

This work was evaluated on two standard large-scale benchmarks including SYNTHIA \rightarrow Cityscapes, GTA5 \rightarrow Cityscapes. We firstly overview the datasets and network architectures in our experiments. Then, the ablation studies will be presented to analyze the performance of CoMaL approach. Finally, we present the quantitative and qualitative results of CoMaL method compared to prior methods on two benchmarks.

A. Dataset Overview and Implementation Details

SYNTHIA (SYNTHIA-RAND-CITYSCAPES) [5] is a synthetic segmentation dataset generated from a virtual world to aid in semantic segmentation of urban settings. It containing 9,400 pixel-level labelled RGB images. There are 16 common classes that overlap with Cityscapes used in the experiments. SYNTHIA is licensed under Creative Commons Attribution-NonCommercial-ShareAlike 3.0.

GTA5 [4], registered under the MIT License, is a collection of 24,966 synthetic, densely labelled images with the resolutions of 1914×1052 pixels. The dataset is collected from a game engine with 33 class categories, using the communication between the game engine and the graphics hardware. There are 19 categories compatible with the Cityscapes [66] used in our experiments.

Cityscapes [66] is a dataset of real-world urban images with 3,975 high-quality, semantic, dense pixel annotations of 30 object classes. The dataset was developed to improve and expand the number of high quality, annotated datasets of urban environments. We use 2,495 images for training and 500 images for testing during our experiments. The license of Cityscapes is made freely available to academic and nonacademic entities for non-commercial purposes.

Implementation We use the DeepLab-V2 [1] architecture with a ResNet-101 [68] backbone for the segmentation network. The Atrous Spatial Pyramid Pooling sampling rate was set

TABLE II
THE EFFECTIVENESS OF OUR PROPOSED BiMAL AND CoMAL LOSSES

Method	Setting	SYNTHIA \rightarrow Cityscapes	GTA5 \rightarrow Cityscapes
ReNet-101	–	33.7	36.6
BiMaL	\mathcal{L}_{llk}	43.9	45.7
BiMaL	$\mathcal{L}_{llk} + \tau$	46.2	47.3
CoMaL	\mathcal{L}_{cls}	54.7	55.4
CoMaL	$\mathcal{L}_{cls} + \mathcal{L}_{CoMaL}$	57.8	59.3

to $\{6, 12, 18, 24\}$. The output of $conv5$ was used to predict the segmentation. The image size is set to 1280×720 . For the experiments with the Transformer backbone, we adopt the MiT-B4 encoder [3] as the backbone similar to [36]. We adopt the structure of [69] for our conditional structure network G . PyTorch [70] was used to implement the framework. We used 4 NVIDIA Quadro P8000 GPUs with 48GB of VRAM each. The Stocahsict Gradient Descent optimizer [71] was used to train the framework with learning rate 2.5×10^{-4} , momentum 0.9, weight decay 10^{-4} , and batch size of 4 per GPU.

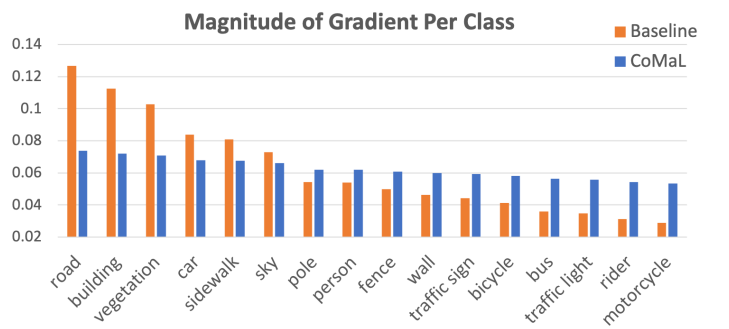


Fig. 7. Normalized Magnitude of Gradients per class.

TABLE III
SEMANTIC SEGMENTATION PERFORMANCE MIoU (%) ON VALIDATION SET OF CITYSCAPES WITH DIFFERENT APPROACHES ON THE RESNET-101 BACKBONE

SYNTHIA → Cityscapes (16 classes). We also show the mIoU (%) of the 13 classes (mIoU*) excluding classes with *.

Models	road	sidewalk	building	wall*	fence*	pole*	light	sign	veg	sky	person	rider	car	bus	mbike	bike	mIoU	mIoU*		
ResNet-101 (without adaptation)	64.9	26.1	71.5	3.0	0.2	21.7	0.1	0.2	73.1	71.0	48.4	20.7	62.9	27.9	12.0	35.6	33.7	39.6		
SPIGAN [26]	71.1	29.8	71.4	3.7	0.3	33.2	6.4	15.6	81.2	78.9	52.7	13.1	75.9	25.5	10.0	20.5	36.8	42.4		
AdaptPatch [6]	82.2	39.4	79.4	-	-	-	6.5	10.8	77.8	82.0	54.9	21.1	67.7	30.7	17.8	32.2	-	46.3		
CLAN [67]	81.3	37.0	80.1	-	-	-	16.1	13.7	78.2	81.5	53.4	21.2	73.0	32.9	22.6	30.7	-	47.8		
AdvEnt [8]	87.0	44.1	79.7	9.6	0.6	24.3	4.8	7.2	80.1	83.6	56.4	23.7	72.7	32.6	12.8	33.7	40.8	47.6		
IntraDA [22]	84.3	37.7	79.5	5.3	0.4	24.9	9.2	8.4	80.0	84.1	57.2	23.0	78.0	38.1	20.3	36.5	41.7	48.9		
DADA [9]	89.2	44.8	81.4	6.8	0.3	26.2	8.6	11.1	81.8	84.0	54.7	19.3	79.7	40.7	14.0	38.8	42.6	49.8		
BiMaL	92.8	51.5	81.5	10.2	1.0	30.4	17.6	15.9	82.4	84.6	55.9	22.3	85.7	44.5	24.6	38.8	46.2	53.7		
MaxSquare [65]	82.9	40.7	80.3	10.2	0.8	25.8	12.8	18.2	82.5	82.2	53.1	18.0	79.0	31.4	10.4	35.6	41.4	48.2		
SAC [19]	89.3	47.3	85.6	26.6	1.3	43.1	45.6	32.0	87.1	89.1	63.7	25.3	87.0	35.6	30.3	52.8	52.6	59.3		
CoMaL	90.5	50.3	85.9	36.0	2.6	45.8	55.3	35.9	89.9	89.9	73.9	28.5	88.4	54.6	42.5	55.3	57.8	64.7		
GTA5 → Cityscapes (19 classes).																				
Models	road	sidewalk	building	wall	fence	pole	light	sign	veg	terrain	sky	person	rider	car	truck	bus	train	mbike	bike	mIoU
ResNet-101 (without adaptation)	75.8	16.8	77.2	12.5	21.0	25.5	30.1	20.1	81.3	24.6	70.3	53.8	26.4	49.9	17.2	25.9	6.5	25.3	36.0	36.6
ROAD [12]	76.3	36.1	69.6	28.6	22.4	28.6	29.3	14.8	82.3	35.3	72.9	54.4	17.8	78.9	27.7	30.3	4.0	24.9	12.6	39.4
AdaptSegNet [7]	86.5	36.0	79.9	23.4	23.3	23.9	35.2	14.8	83.4	33.3	75.6	58.5	27.6	73.7	32.5	35.4	3.9	30.1	28.1	42.4
MinEnt [8]	84.2	25.2	77.0	17.0	23.3	24.2	33.3	26.4	80.7	32.1	78.7	57.5	30.0	77.0	37.9	44.3	1.8	31.4	36.9	43.1
AdvEnt [8]	89.9	36.5	81.6	29.2	25.2	28.5	32.3	22.4	83.9	34.0	77.1	57.4	27.9	83.7	29.4	39.1	1.5	28.4	23.3	43.8
IntraDA [22]	90.6	36.1	82.6	29.5	21.3	27.6	31.4	23.1	85.2	39.3	80.2	59.3	29.4	86.4	33.6	53.9	0.0	32.7	37.6	46.3
BiMaL	91.2	39.6	82.7	29.4	25.2	29.6	34.3	25.5	85.4	44.0	80.8	59.7	30.4	86.6	38.5	47.6	1.2	34.0	36.8	47.3
MaxSquare [65]	89.4	43.0	82.1	30.5	21.3	30.3	34.7	24.0	85.3	39.4	78.2	63.0	22.9	84.6	36.4	43.0	5.5	34.7	33.5	46.4
SAC [19]	90.3	53.9	86.6	42.5	27.4	45.1	48.6	42.9	87.5	40.2	86.0	67.6	29.7	88.5	49.0	54.6	9.8	26.6	45.1	53.8
CoMaL	90.6	58.7	87.9	44.1	44.4	47.3	54.1	52.9	88.7	47.1	87.4	70.6	39.7	88.8	55.3	58.7	8.7	47.7	54.4	59.3

B. Ablation Study

Structural Learning with Conditional Structure Network

This experiment illustrates the capability of the structural

TABLE IV
SEMANTIC SEGMENTATION PERFORMANCE MIoU (%) ON VALIDATION SET OF CITYSCAPES WITH DIFFERENT APPROACHES ON THE TRANSFORMER BACKBONE.

Models	road	sidewalk	building	wall*	fence*	pole*	light	sign	veg	terrain	sky	person	rider	car	bus	mbike	bike	mIoU	mIoU*	
SYNTHIA → Cityscapes (16 classes). We also show the mIoU (%) of the 13 classes (mIoU*) excluding classes with *.																				
Swin-S [37] (without adaptation)	30.6	26.1	42.9	3.8	0.1	25.9	32.3	15.6	80.3	70.7	60.5	8.2	69.0	30.3	11.2	12.3	32.5	37.7		
Swin-B [37] (without adaptation)	57.3	33.8	56.0	6.3	0.2	33.8	35.5	18.9	79.9	74.8	63.1	10.9	78.3	39.0	20.8	19.4	39.2	45.2		
TransDA-S [37]	82.1	40.9	86.2	25.8	1.0	53.0	53.7	36.1	89.2	90.3	68.0	26.2	90.9	58.4	41.2	45.4	55.5	62.2		
TransDA-B [37]	90.4	54.8	86.4	31.1	1.7	53.8	61.1	37.1	90.3	93.0	71.2	25.3	92.3	66.0	44.4	49.8	59.3	66.3		
DAFormer [36]	84.5	40.7	88.4	41.5	6.5	50.0	55.0	54.6	86.0	89.8	73.2	48.2	87.2	53.2	53.9	61.7	60.9	67.4		
BiMaL	86.9	48.1	88.4	40.2	8.2	50.2	55.2	52.7	85.5	91.0	72.2	48.7	87.4	60.3	54.8	61.7	62.0	68.7		
CoMaL	90.5	50.3	88.5	40.4	8.2	50.3	55.3	52.8	89.9	91.1	73.9	49.3	88.4	61.1	55.4	62.8	63.0	69.9		
GTA5 → Cityscapes (19 classes).																				
Models	road	sidewalk	building	wall	fence	pole	light	sign	veg	terrain	sky	person	rider	car	truck	bus	train	mbike	bike	mIoU
Swin-S [37] (without adaptation)	55.9	21.8	63.1	14.0	22.0	27.2	46.8	17.4	83.3	32.8	86.1	62.2	28.7	43.8	32.2	36.9	1.1	34.8	35.5	39.2
Swin-B [37] (without adaptation)	63.3	28.6	68.3	16.8	23.4	37.8	51.0	34.3	83.8	42.1	85.7	68.5	25.4	83.5	36.3	17.7	2.9	36.1	42.3	44.6
TransDA-S [37]	92.9	59.1	88.2	42.5	32.0	47.6	57.6	39.2	89.6	42.0	94.1	74.3	45.3	91.4	54.0	58.0	44.4	48.3	51.4	60.6
TransDA-B [37]	94.7	64.2	89.2	48.1	45.8	50.1	60.2	40.8	90.4	50.2	93.7	76.7	47.6	92.5	56.8	60.1	47.6	49.6	55.4	63.9
DAFormer [36]	95.7	70.2	89.4	53.5	48.1	49.6	55.8	59.4	89.9	47.9	92.5	72.2	44.7	92.3	74.5	78.2	65.1	55.9	61.8	68.3
BiMaL	96.1	72.0	89.3	52.4	48.1	48.7	56.2	61.0	89.5	46.4	92.3	72.0	46.1	91.9	67.4	80.9	67.7	54.4	61.7	68.1
CoMaL	96.7	74.8	89.5	55.2	48.3	50.6	56.3	63.6	90.0	49.0	92.6	72.0	46.3	92.6	80.1	81.0	70.1	57.7	63.4	70.0

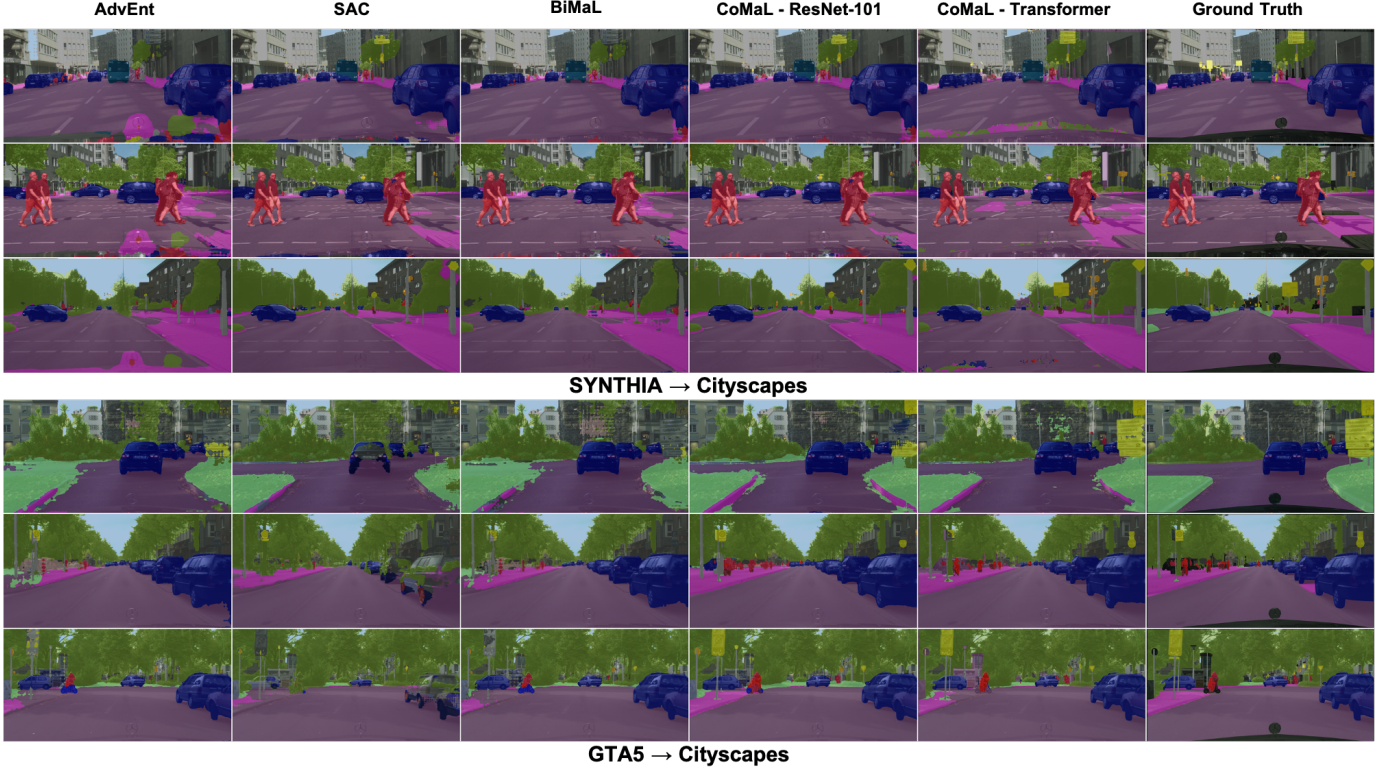


Fig. 8. **Qualitative Results.** We compare our results, i.e., BiMaL, CoMaL with the ResNet-101 backbone, and CoMaL with the Transformer backbone, with AdvEnt [8], SAC [19], (a) SYNTHIA → Cityscapes and (b) GTA5 → Cityscapes (Best view in color).

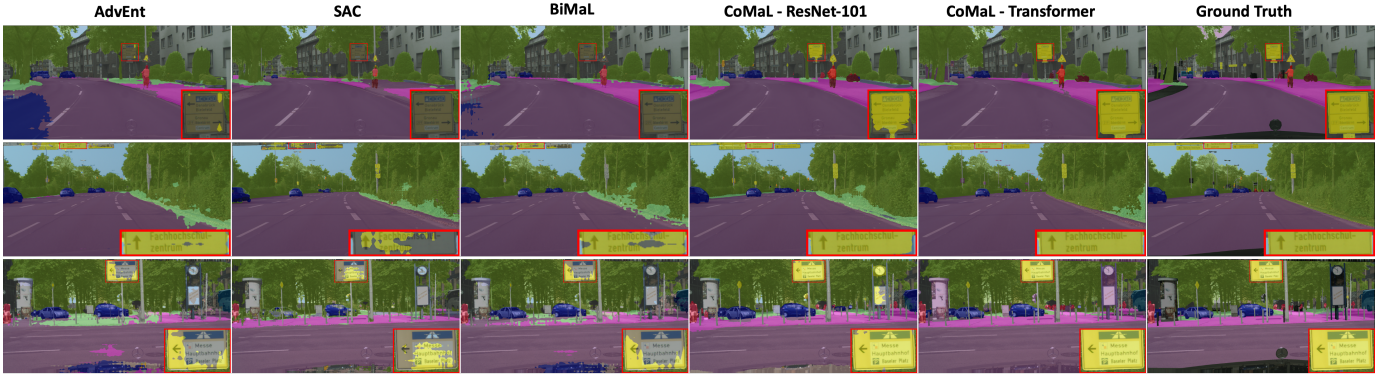


Fig. 9. **Qualitative Results of Long-tail Classes.** We highlight the long-tail class (i.e., traffic sign) and compare the results of AdvEnt [8], SAC [19], BiMaL, CoMaL with the ResNet-101 backbone, and CoMaL with the Transformer backbone.

condition modeling of the generative network G trained on GTA5. As in Fig. 6(a), our structural condition network can capture the structure information of the segmentation. In particular, at the detail level of the segmentation, the structural borders between objects are well modeled. Moreover, as in Fig. 6(b), our conditional network G is able to model the segmentation conditioned on the given objects. This experiment has confirmed that our approach can sufficiently model the segmentation even with complex and diverse structures as scene segmentation.

Effectiveness of Losses Table II reports the mIoU performance of our proposed BiMaL and CoMaL losses compared to the baseline of ResNet-101. In BiMaL experiments, we

consider three cases: (1) without adaptation (train with source only), (2) BiMaL without regularization term ($\mathcal{L}_{lik}(\mathbf{y})$ only), and (3) BiMaL with regularization term ($\mathcal{L}_{lik}(\mathbf{y}) + \tau(\mathbf{y})$). Overall, the proposed BiMaL improve the performance of the method. In particular, the mIoU accuracy of the baseline (without adaptation) is 33.7% and 36.6%. In comparison, BiMaL without regularization and BiMaL with regularization achieve the mIoU accuracy of 43.5% and 46.2% on SYNTHIA → Cityscapes, and 46.2% and 47.3% on GTA5 → Cityscapes, respectively. In CoMaL experiments, we deploy only the conditional class-weighted loss (\mathcal{L}_{cls}), the performance of CoMaL are improved up to 54.7% and 55.4% on the benchmarks of SYNTHIA → Cityscapes and GTA5 → Cityscapes,

respectively. Moreover, when we utilize both class-weighted loss and conditional maximum likelihood loss (\mathcal{L}_{CoMaL}), the performance of our proposals improves by a large margin and achieves the mIoU up to 57.8% on SYNTHIA → Cityscapes and 59.3% on GTA5 → Cityscapes.

Effectiveness of Gradients We visualize the effect of gradients updated to each class by taking a subset of the validation set of Cityscapes to compute and average the gradients of predictions with respect to each class. Fig. 7 illustrates the normalized magnitude of gradients with respect to each class. The gradients of each class produced by our method have fairly updated with the predictions. . Meanwhile, without CoMaL, the gradients updated to the predictions of head class largely dominate the tailed classes.

C. Quantitative and Qualitative Results

In this experiment, we compare our CoMaL with prior SOTA methods on two benchmarks: SYNTHIA → Cityscapes and GTA5 → Cityscapes. As other standard benchmarks [8], [19], the performance of segmentation is compared by the mean Intersection over Union (mIoU) metric.

SYNTHIA → Cityscapes: Table III presents the our SOTA performance of the proposed BiMaL and CoMaL approach compared to prior methods on the ReNet-101 backbone over 16 common classes on the Cityscape validation set. In the BiMaL experimental setting, we have compared our BiMaL results with prior approaches in which the long-tail issue has been not aware. Our proposed BiMaL achieves better accuracy than the prior methods, i.e. 46.2% higher than DADA [9] by 3.6%. Considering per-class results, our method significantly improves the results on classes of ‘sidewalk’ (51.5%), ‘car’ (85.7%), and ‘bus’ (44.5%). Meanwhile, in the experimental setting of CoMaL in which the long-tail issue has been taken in to account, our CoMaL approach achieved higher than the previous SOTA method (SAC) [19] by 5.2%. Considering the per class result, in comparison with SAC [19], our method can significantly improve the results on the tailed classes, e.g. ‘bus’ (+19.0%), ‘motorbike’ (+12.2%), ‘person’ (+10.2%), ‘traffic light’ (+9.7%), ‘wall’ (+9.4%), etc. In addition, our approach maintains and improves the performance of the head class compared to SAC [19], i.e ‘road’ (90.5%), ‘building’ (85.9%), ‘vegetation’ (89.9%), ‘car’ (88.4%), ‘sidewalk’ (50.3%), ‘sky’ (89.9%). We also report the results on a 13-class subset where our proposed method also achieves the State-of-the-Art performance. Additionally, we have reported our results trained on Transformer backbone as reported in Table IV. In this experiment, we also achieve the state-of-the-art performance compared with prior approaches trained on Transformer backbone.

GTA5 → Cityscapes: Table III illustrates the mIoU accuracy over 19 classes of Cityscapes. Overall, our CoMaL approach achieves the mIoU accuracy of 59.3% that is the SOTA performance compared to the prior methods on the same ResNet-101 backbone. In the BiMaL experimental setting, our BiMaL approach achieved mIoU of 47.3% that is SOTA performance compared to the previous methods. Analysing per-class results, our method gains the improvement on most

classes, e.g., the results on classes of ‘terrain’ (+10.0%), ‘truck’ (+9.1%), ‘bus’ (+8.0%), ‘motorbike’ (+5.6%) show significant improvements compared to AdvEnt. Meanwhile, in the CoMaL experimental setting, further analysis suggests that our method achieves comparable results and improves the performance of segmentation on the tail classes. In particular, the results on the tail classes of “terrain”, “fence”, “traffic sign”, “bicycle”, “truck”, “rider”, and “motorcycle” have been improved by 6.9%, 17.0%, 10.0%, 9.3%, 6.3%, 10.0%, and 21.1%, respectively. Furthermore, the performance of the head classes are maintained and improved, i.e. the mIoU results of “road”, “building”, “vegetation”, “car”, and “sky” are 90.6%, 87.9%, 88.7%, 88.8%, and 87.4%, respectively. Also, we have achieved the state-of-the-art performance and compared our results with prior approaches trained on the Transformer backbone as reported in Table IV.

Qualitative Results: As shown in Fig. 8, our approach produces better qualitative results compared to prior SOTA approaches, , i.e. AdvEnt [8], BiMaL , DA-SAC [19], BiMaL, CoMaL with the ResNet-101 backbone, and CoMaL with the Transformer backbone. The most distinguishable improvements come from the tail classes that occupy smaller portions of a given image. In particular, the segmentation of instances occupying tail classes such as signs, people, and poles are more clearly defined. The model is able to accurately identify the border regions of these classes. Figure 9 highlights our segmentation results on long-tail classes compared to other approaches. The continuity of each instance more clearly matches the ground truth labels, as the model does not leave out as many parts of the smaller objects. It is able to cohesively segment the tail classes, reducing the portion of each tail-class that is incorrectly labeled, while also recognizing where it begins and ends. Moreover, the head classes are qualitatively maintained and enhanced along with the tail classes. Although there is little noise in the head classes, the boundaries are still precise and match the ground truth.

VI. CONCLUSIONS

This paper has presented a novel metric for cross-domain long-tail adaptation in semantic segmentation. A new structural condition network has been introduced to learn the spatial relationship and structure information of the segmentation. Further, conditional maximum likelihood losses have been derived to tackle the issues of long-tail distributions that occur in both domains. The intensive experiments on two benchmarks, i.e., SYNTHIA → Cityscapes, GTA → Cityscapes, have shown the performance of our CoMaL approach. The method achieves the SOTA performance in both benchmarks and improves the performance of the segmentation on tailed class, while also maintaining and improving the mIoU results on head classes.

REFERENCES

- [1] L.-C. Chen, G. Papandreou, I. Kokkinos, K. Murphy, and A. L. Yuille, “Deeplab: Semantic image segmentation with deep convolutional nets, atrous convolution, and fully connected CRFs,” *TPAMI*, 2018.
- [2] L.-C. Chen, G. Papandreou, F. Schroff, and H. Adam, “Rethinking atrous convolution for semantic image segmentation,” *arXiv preprint arXiv:1706.05587*, 2017.

[3] E. Xie, W. Wang, Z. Yu, A. Anandkumar, J. M. Alvarez, and P. Luo, “Segformer: Simple and efficient design for semantic segmentation with transformers,” in *NeurIPS*, 2021.

[4] S. R. Richter, V. Vineet, S. Roth, and V. Koltun, “Playing for data: Ground truth from computer games,” in *ECCV*, 2016.

[5] G. Ros, L. Sellart, J. Materzynska, D. Vazquez, and A. M. Lopez, “The SYNTHIA dataset: A large collection of synthetic images for semantic segmentation of urban scenes,” in *CVPR*, 2016.

[6] Y.-H. Tsai, K. Sohn, S. Schulter, and M. Chandraker, “Domain adaptation for structured output via discriminative representations,” *arXiv:1901.05427*, 2019.

[7] Y.-H. Tsai, W.-C. Hung, S. Schulter, K. Sohn, M.-H. Yang, and M. Chandraker, “Learning to adapt structured output space for semantic segmentation,” in *CVPR*, 2018.

[8] T.-H. Vu, H. Jain, M. Bucher, M. Cord, and P. Pérez, “Advent: Adversarial entropy minimization for domain adaptation in semantic segmentation,” in *CVPR*, 2019.

[9] —, “Dada: Depth-aware domain adaptation in semantic segmentation,” in *ICCV*, 2019.

[10] Y. Ganin and V. Lempitsky, “Unsupervised domain adaptation by backpropagation,” in *ICML*, 2015.

[11] M. Long, Y. Cao, J. Wang, and M. I. Jordan, “Learning transferable features with deep adaptation networks,” in *ICML*, 2015.

[12] Y. Chen, W. Li, and L. Van Gool, “Road: Reality oriented adaptation for semantic segmentation of urban scenes,” in *CVPR*, 2018.

[13] J. Hoffman, E. Tzeng, T. Park, J.-Y. Zhu, P. Isola, K. Saenko, A. Efros, and T. Darrell, “CyCADA: Cycle-consistent adversarial domain adaptation,” in *ICML*, 2018.

[14] W. Hong, Z. Wang, M. Yang, and J. Yuan, “Conditional generative adversarial network for structured domain adaptation,” in *CVPR*, 2018.

[15] E. Tzeng, J. Hoffman, K. Saenko, and T. Darrell, “Adversarial discriminative domain adaptation,” in *CVPR*, 2017.

[16] X. Yue, Z. Zheng, S. Zhang, Y. Gao, T. Darrell, K. Keutzer, and A. S. Vincentelli, “Prototypical cross-domain self-supervised learning for few-shot unsupervised domain adaptation,” in *CVPR*, 2021.

[17] G. Kang, L. Jiang, Y. Yang, and A. G. Hauptmann, “Contrastive adaptation network for unsupervised domain adaptation,” in *CVPR*, 2019.

[18] P. Zhang, B. Zhang, T. Zhang, D. Chen, Y. Wang, and F. Wen, “Prototypical pseudo label denoising and target structure learning for domain adaptive semantic segmentation,” *arXiv preprint arXiv:2101.10979*, 2021.

[19] N. Araslanov, , and S. Roth, “Self-supervised augmentation consistency for adapting semantic segmentation,” in *Proceedings of the IEEE Conference on Computer Vision and Pattern Recognition (CVPR)*, 2021.

[20] Y. Zou, Z. Yu, B. V. Kumar, and J. Wang, “Unsupervised domain adaptation for semantic segmentation via class-balanced self-training,” in *ECCV*, 2018.

[21] J. Hoffman, D. Wang, F. Yu, and T. Darrell, “FCNs in the wild: Pixel-level adversarial and constraint-based adaptation,” *arXiv:1612.02649*, 2016.

[22] F. Pan, I. Shin, F. Rameau, S. Lee, and I. S. Kweon, “Unsupervised intra-domain adaptation for semantic segmentation through self-supervision,” in *CVPR*, 2020.

[23] T.-D. Truong, C. N. Duong, N. Le, S. L. Phung, C. Rainwater, and K. Luu, “Bimal: Bijective maximum likelihood approach to domain adaptation in semantic scene segmentation,” in *ICCV*, 2021.

[24] J. Wang, W. Zhang, Y. Zang, Y. Cao, J. Pang, T. Gong, K. Chen, Z. Liu, C. C. Loy, and D. Lin, “Seesaw loss for long-tailed instance segmentation,” in *Proceedings of the IEEE Conference on Computer Vision and Pattern Recognition*, 2021.

[25] T.-I. Hsieh, E. Robb, H.-T. Chen, and J.-B. Huang, “Droploss for long-tail instance segmentation,” in *Proceedings of the Workshop on Artificial Intelligence Safety 2021 co-located with the Thirty-Fifth AAAI Conference on Artificial Intelligence*, 2021.

[26] K.-H. Lee, G. Ros, J. Li, and A. Gaidon, “SPIGAN: Privileged adversarial learning from simulation,” in *ICLR*, 2019.

[27] M. Chen, H. Xue, and D. Cai, “Domain adaptation for semantic segmentation with maximum squares loss,” in *ICCV*, 2019.

[28] Y.-H. Chen, W.-Y. Chen, Y.-T. Chen, B.-C. Tsai, Y.-C. F. Wang, and M. Sun, “No more discrimination: Cross city adaptation of road scene segmenters,” in *ICCV*, 2017.

[29] Z. Murez, S. Kolouri, D. Kriegman, R. Ramamoorthi, and K. Kim, “Image to image translation for domain adaptation,” in *CVPR*, 2018.

[30] J.-Y. Zhu, T. Park, P. Isola, and A. A. Efros, “Unpaired image-to-image translation using cycle-consistent adversarial networks,” in *ICCV*, 2017.

[31] J. Long, E. Shelhamer, and T. Darrell, “Fully convolutional networks for semantic segmentation,” in *CVPR*, 2015.

[32] G. Lin, A. Milan, C. Shen, and I. Reid, “Refinenet: Multi-path refinement networks for high-resolution semantic segmentation,” in *CVPR*, 2017.

[33] T. Pohlen, A. Hermans, M. Mathias, and B. Leibe, “Full-resolution residual networks for semantic segmentation in street scenes,” in *CVPR*, 2017.

[34] F. Yu and V. Koltun, “Multi-scale context aggregation by dilated convolutions,” in *ICLR*, Y. Bengio and Y. LeCun, Eds., 2016.

[35] L.-C. Chen, Y. Zhu, G. Papandreou, F. Schroff, and H. Adam, “Encoder-decoder with atrous separable convolution for semantic image segmentation,” in *ECCV*, 2018.

[36] L. Hoyer, D. Dai, and L. Van Gool, “DAFormer: Improving network architectures and training strategies for domain-adaptive semantic segmentation,” in *CVPR*, 2022.

[37] R. Chen, Y. Rong, S. Guo, J. Han, F. Sun, T. Xu, and W. Huang, “Smoothing matters: Momentum transformer for domain adaptive semantic segmentation,” *CoRR*, 2022.

[38] X. Zhu, H. Zhou, C. Yang, J. Shi, and D. Lin, “Penalizing top performers: Conservative loss for semantic segmentation adaptation,” in *ECCV*, 2018.

[39] Z. Wu, X. Han, Y.-L. Lin, M. Gokhan Uzunbas, T. Goldstein, S. Nam Lim, and L. S. Davis, “DCAN: Dual channel-wise alignment networks for unsupervised scene adaptation,” in *ECCV*, 2018.

[40] C. Sakaridis, D. Dai, S. Hecker, and L. Van Gool, “Model adaptation with synthetic and real data for semantic dense foggy scene understanding,” in *ECCV*, 2018.

[41] V. Vapnik and A. Vashist, “A new learning paradigm: Learning using privileged information,” *Neural networks*, 2009.

[42] J. Hoffman, S. Gupta, and T. Darrell, “Learning with side information through modality hallucination,” in *CVPR*, 2016.

[43] D. Lopez-Paz, L. Bottou, B. Schölkopf, and V. Vapnik, “Unifying distillation and privileged information,” in *ICLR*, 2016.

[44] T. Mordan, N. Thome, G. Henaff, and M. Cord, “Revisiting multi-task learning with rock: a deep residual auxiliary block for visual detection,” in *NIPS*, 2018.

[45] V. Sharmanska, N. Quadrianto, and C. H. Lampert, “Learning to rank using privileged information,” in *ICCV*, 2013.

[46] Y. Grandvalet and Y. Bengio, “Semi-supervised learning by entropy minimization,” in *NIPS*, 2005.

[47] J. T. Springenberg, “Unsupervised and semi-supervised learning with categorical generative adversarial networks,” *ICLR*, 2016.

[48] Z. Yan, X. Yu, Y. Qin, Y. Wu, X. Han, and S. Cui, *Pixel-Level Intra-Domain Adaptation for Semantic Segmentation*. Association for Computing Machinery, 2021.

[49] X. Li, Q. Sun, Y. Liu, Q. Zhou, S. Zheng, T.-S. Chua, and B. Schiele, “Learning to self-train for semi-supervised few-shot classification,” in *NeurIPS*, 2019.

[50] Z. Liu, Z. Miao, X. Zhan, J. Wang, B. Gong, and S. X. Yu, “Large-scale long-tailed recognition in an open world,” 2019.

[51] J. Ren, C. Yu, S. Sheng, X. Ma, H. Zhao, S. Yi, and H. Li, “Balanced meta-softmax for long-tailed visual recognition,” 2020.

[52] L. Dinh, D. Krueger, and Y. Bengio, “Nice: Non-linear independent components estimation,” 2015.

[53] L. Dinh, J. Sohl-Dickstein, and S. Bengio, “Density estimation using real nvp,” 2017.

[54] C. Nhan Duong, K. Gia Quach, K. Luu, N. Le, and M. Savvides, “Temporal non-volume preserving approach to facial age-progression and age-invariant face recognition,” in *ICCV*, Oct 2017.

[55] C. N. Duong, T.-D. Truong, K. Luu, K. G. Quach, H. Bui, and K. Roy, “Vec2face: Unveil human faces from their blackbox features in face recognition,” in *CVPR*, 2020.

[56] D. P. Kingma and P. Dhariwal, “Glow: Generative flow with invertible 1x1 convolutions,” in *NIPS*, S. Bengio, H. Wallach, H. Larochelle, K. Grauman, N. Cesa-Bianchi, and R. Garnett, Eds., 2018.

[57] C. N. Duong, K. G. Quach, K. Luu, T. H. N. Le, M. Savvides, and T. D. Bui, “Learning from longitudinal face demonstration—where tractable deep modeling meets inverse reinforcement learning,” *IJCV*, 2019.

[58] T.-D. Truong, C. N. Duong, M.-T. Tran, N. Le, and K. Luu, “Fast flow reconstruction via robust invertible $n \times n$ convolution,” *Future Internet*, 2021.

[59] C. N. Duong, K. Luu, K. G. Quach, N. Nguyen, E. Patterson, T. D. Bui, and N. Le, “Automatic face aging in videos via deep reinforcement learning,” in *CVPR*, 2019.

[60] C. N. Duong, K. Luu, K. G. Quach, and T. D. Bui, “Longitudinal face modeling via temporal deep restricted boltzmann machines,” in *CVPR*, 2016.

- [61] ——, “Deep appearance models: A deep boltzmann machine approach for face modeling,” *IJCV*, 2019.
- [62] T.-D. Truong, C. N. Duong, K. Luu, M.-T. Tran, and N. Le, “Domain generalization via universal non-volume preserving approach,” in *CRV*, 2020.
- [63] A. van den Oord, N. Kalchbrenner, and K. Kavukcuoglu, “Pixel recurrent neural networks,” 2016.
- [64] J. L. Ba, J. R. Kiros, and G. E. Hinton, “Layer normalization,” 2016.
- [65] M. Chen, H. Xue, and D. Cai, “Domain adaptation for semantic segmentation with maximum squares loss,” in *ICCV*, 2019.
- [66] M. Cordts, M. Omran, S. Ramos, T. Rehfeld, M. Enzweiler, R. Benenson, U. Franke, S. Roth, and B. Schiele, “The Cityscapes dataset for semantic urban scene understanding,” in *CVPR*, 2016.
- [67] Y. Luo, L. Zheng, T. Guan, J. Yu, and Y. Yang, “Taking a closer look at domain shift: Category-level adversaries for semantics consistent domain adaptation,” *arXiv:1809.09478*, 2019.
- [68] K. He, X. Zhang, S. Ren, and J. Sun, “Deep residual learning for image recognition,” 2015.
- [69] M. Chen, A. Radford, R. Child, J. Wu, H. Jun, P. Dhariwal, D. Luan, and I. Sutskever, “Generative pretraining from pixels,” *ICML*, 2020.
- [70] A. Paszke, S. Gross, F. Massa, A. Lerer, J. Bradbury, G. Chanan, T. Killeen, Z. Lin, N. Gimelshein, L. Antiga, A. Desmaison, A. Kopf, E. Yang, Z. DeVito, M. Raison, A. Tejani, S. Chilamkurthy, B. Steiner, L. Fang, J. Bai, and S. Chintala, “Pytorch: An imperative style, high-performance deep learning library,” 2019.
- [71] L. Bottou, “Large-scale machine learning with stochastic gradient descent,” in *in COMPSTAT*, 2010.



Chi Nhan Duong is currently a Senior Technical Staff and having research collaborations with both Computer Vision and Image Understanding (CVIU) Lab, University of Arkansas, USA and Concordia University, Montreal, Canada. He had been a Research Associate in Cylab Biometrics Center at Carnegie Mellon University (CMU), USA since September 2016. He received his Ph.D. degree in Computer Science with the Department of Computer Science and Software Engineering, Concordia University, Montreal, Canada. He was an Intern with National Institute of Informatics, Tokyo Japan in 2012. He received his B.S. and M.Sc. degrees in Computer Science from the Department of Computer Science, Faculty of Information Technology, University of Science, Ho Chi Minh City, Vietnam, in 2008 and 2012, respectively. His research interests include Deep Generative Models, Face Recognition in surveillance environments, Face Aging in images and videos, Biometrics, and Digital Image Processing, and Digital Image Processing (denoising, inpainting and super-resolution). He is currently a reviewer of several top-tier journals including IEEE Transaction on Pattern Analysis and Machine Intelligence (TPAMI), IEEE Transaction on Image Processing (TIP), Journal of Signal Processing, Journal of Pattern Recognition, Journal of Pattern Recognition Letters. He is also recognized as an outstanding reviewer of several top-tier conferences such as The IEEE Computer Vision and Pattern Recognition (CVPR), International Conference on Computer Vision (ICCV), European Conference On Computer Vision (ECCV), Conference on Neural Information Processing Systems (NeurIPS), International Conference on Learning Representations (ICLR) and the AAAI Conference on Artificial Intelligence. He is also a Program Committee Member of Precognition: Seeing through the Future, CVPR.



Thanh-Dat Truong is currently a Ph.D. Candidate at the Department of Computer Science and Computer Engineering of the University of Arkansas. He received his B.Sc. degree in Computer Science from Honors Program, University of Science, VNU in 2019. He was a research intern at Coordinated Lab Science at the University of Illinois at Urbana-Champaign in 2018. When Thanh-Dat Truong was an undergraduate student, he worked as a research assistant at Artificial Intelligence Lab at the University of Science, VNU. Thanh-Dat Truong’s research

interests widely include Face Recognition, Action Recognition, Domain Adaptation, Deep Generative Model, Adversarial Learning. His papers appear at top tier conferences such as Computer Vision and Pattern Recognition, International Conference on Computer Vision, International Conference on Pattern Recognition, Canadian Conference on Computer and Robot Vision. He is also a reviewer of top-tier journals and conferences including IEEE Transaction on Pattern Analysis and Machine Intelligence, IEEE Transaction on Image Processing, Journal of Computers Environment and Urban Systems, IEEE Access, Computer Vision and Pattern Recognition, European Conference on Computer Vision, Asian Conference on Computer Vision, Winter Conference on Applications of Computer Vision, International Conference on Pattern Recognition.



Pierce Helton is an undergraduate student in the Department of Computer Science and Computer Engineering at the University of Arkansas. He is expected to graduate in Fall of 2022. He is currently working in the Computer Vision and Image Understanding lab at his university. His research interests are Machine Learning, Deep Learning, and Computer Vision. Pierce has plans to work in the industry and potentially pursue a M.S. in Computer Science after earning his B.S.



Ashley Dowling is currently a Professor in the Department of Entomology and Plant Pathology at the University of Arkansas. He is serving as Editor-in-Chief of the International Journal of Acarology. His research interests focus on biodiversity, evolutionary biology, and ecology of insects and other arthropods. He has coauthored 80+ papers in journals on these topics and trained more than 20 graduate students.



Xin Li (Fellow, IEEE) received the B.S. (Hons.) degree in electronic engineering and information science from the University of Science and Technology of China, Hefei, China, in 1996, and the Ph.D. degree in electrical engineering from Princeton University, Princeton, NJ, USA, in 2000. From 2000 to 2002, he was a Technical Staff Member with the Sharp Laboratories of America, Camas, WA, USA. Since 2003, he has been a Faculty Member with the Lane Department of Computer Science and Electrical Engineering. His research interests

include image/video coding and processing. He was the recipient of the Best Student Paper Award at the Conference of Visual Communications and Image Processing in 2001, Best Student Paper Award at the IEEE Asilomar Conference on Signals, Systems and Computers in 2006, and Best Paper Award at the Conference of Visual Communications and Image Processing in 2010. He is currently a Member of the Image, Video, and Multidimensional Signal Processing Technical Committee and an Associate Editor for the IEEE Transactions on Circuits and Systems for Video Technology.



Khoa Luu is currently an Assistant Professor and the Director of Computer Vision and Image Understanding (CVIU) Lab in Department of Computer Science & Computer Engineering at University of Arkansas. He is serving as an Associate Editor of IEEE Access journal. He was the Research Project Director in Cylab Biometrics Center at Carnegie Mellon University (CMU), USA. He has received four patents and two best paper awards, and coauthored 120+ papers in conferences and journals. He was a vice chair of Montreal Chapter IEEE SMCS in

Canada from September 2009 to March 2011. His research expertise includes Biometrics, Face Recognition, Tracking, Human Behavior Understanding, Scene Understanding, Domain Adaptation, Deep Generative Modeling, Image and Video Processing, Deep Learning, Compressed Sensing and Quantum Machine Learning. He is a co-organizer and a chair of CVPR Precognition Workshop in 2019, 2020, 2021, 2022; MICCAI Workshop in 2019, 2020 and ICCV Workshop in 2021. He is a PC member of AAAI, ICPRAI in 2020, 2022. He has been an active reviewer for several AI conferences and journals, such as CVPR, ICCV, ECCV, NeurIPS, ICLR, IEEE-TPAMI, IEEE-TIP, IEEE Access, Journal of Pattern Recognition, Journal of Image and Vision Computing, Journal of Signal Processing, and Journal of Intelligence Review.